The Glucose Transporter 2 regulates CD8+ T cell function via environment sensing.

Hongmei Fu[1†], Juho Vuononvirta[1†], Silvia Fanti[1], Fabrizia Bonacina[2], Antonio D'Amati[3], Guosu Wang[1], Thanushiyan Poobalasingam[1], Maria Fankhaenel[4], Davide Lucchesi[1], Rachel Coleby[1], David Tarussio[5], Bernard Thorens[5], Robert J. Hearnden[4], M. Paula Longhi[1], Paul Grevitt[4], Madeeha H. Sheikh[1], Egle Solito[1], Susana Godinho[4], Michele Bombardieri[1], David M. Smith[6], Dianne Cooper[1], Asif Iqbal[7], Jeffrey C. Rathmell[8], Samuel Schaefer[8], Valle Morales[4], Katiuscia Bianchi[4], Giuseppe Danilo Norata[2], and Federica M. Marelli-Berg[1*].

[1]William Harvey Research Institute, Faculty of Medicine and Dentistry, Queen Mary University of London, Charterhouse Square, London EC1M 6BQ, UK.

[2]Department of Pharmacological and Biomolecular Sciences (DisFeB), Università Degli Studi di Milano, Milan, 20133, Italy.

[3]Section of Anatomical Pathology Department of Precision and Regenerative Medicine, University of Bari Medical School, 70124 Bari, Italy

[4]Bart's Cancer Institute, Faculty of Medicine and Dentistry, Queen Mary University of London, Charterhouse Square, London EC1M 6BQ, UK.

[5]Faculty of Biology and Medicine, Center for Integrative Genomics, Génopode Building - UNIL Sorge, CH-1015, University of Lausanne, Switzerland

[6]Discovery Sciences, Innovative Medicines and Early Development Biotech Unit, AstraZeneca, Cambridge, Cambridgeshire CB40WG, UK.

[7]Institute of Cardiovascular Sciences, University of Birmingham, Birmingham B15 2TT, UK

[8]Department of Pathology, Microbiology, and Immunology, Vanderbilt Center for Immunobiology, Vanderbilt University Medical Center, Nashville, TN 37232, USA

***Correspondence:** f.marelli-berg@qmul.ac.uk

† Equal contribution

Abstract

T cell activation is associated with a profound and rapid metabolic response to meet increased energy demands for cell division, differentiation, and development of effector function. Glucose uptake and engagement of the glycolytic pathway are major checkpoints for this event. Here we show that the low affinity, concentration-dependent glucose transporter 2 (Glut2) regulates the development of CD8+ T cell effector responses by promoting glucose uptake, glycolysis and glucose storage. Expression of Glut2 is modulated by environmental factors including glucose and oxygen availability and extracellular acidification. Glut2 is highly expressed by circulating, recently primed T cells, allowing efficient glucose uptake and storage. In glucose-deprived inflammatory environments Glut2 becomes downregulated, thus preventing passive loss of intracellular glucose. Mechanistically, Glut2 expression is regulated by a combination of molecular interactions involving HIF1α, Galectin-9 and Stomatin. Finally, we show that human T cells also rely on this glucose transporter, thus providing a potential target for therapeutic immunomodulation.

One Sentence Summary

By sensing glucose and oxygen availability, the Glucose Transporter 2 regulates CD8+ T cell metabolism and function.

INTRODUCTION

Different T cells adapt metabolic pathways to their specific functions. Quiescent naïve T cells uptake low levels of glucose and rely primarily on fatty acid oxidation and basal glycolysis to maintain cellular ATP levels through mitochondrial oxidative phosphorylation [1]. Upon antigen encounter, T cells switch to glycolytic energy production and increased biosynthesis, which allow them to divide and differentiate. T cell differentiation into specialized helper/cytotoxic (Th/Tc) subsets enables the immune system to respond appropriately to a huge variety of pathogens [2]. CD8+ T cells proliferate more rapidly and differentiate into cytotoxic CD8+ T cells producing inflammatory cytokines such as IFN-γ to target and kill infected and transformed cells [3]. Specific metabolic adaptations associated with distinct T cell subsets have been related to their function in the immune response [4]. CD8+ T cell primary and secondary responses are strongly associated with engagement of the glycolytic pathway [5].

Glucose uptake by T cells is a key metabolic checkpoint, which provides substrate through the facilitated diffusion glucose transporters (Gluts). Glut family members are differentially regulated, have distinct amino acid sequences, substrate specificities, kinetic properties and tissue and cellular localizations [6, 7]. Gluts can be divided into subclasses. Class I facilitative Gluts include Glut1, Glut2, Glut3 and Glut4 [6, 7].

Glut1 is a high-affinity glucose transporter with a Km for glucose of around 3-7 mM and has been proposed as the primary glucose transporter of T cells [8]. Cell surface expression of Glut1 is nearly undetectable in quiescent T cells, but it becomes strongly upregulated to fuel glycolysis upon activation [9-11]. However, studies with Glut1-deficient mice have shown that glycolytic CD8+ T cells are less dependent on Glut1 compared to their CD4-expressing counterpart [12], suggesting the other Gluts might support efficient glucose uptake in the CD8+ T cell subset.

Glut2 has a uniquely low affinity ($K_m \sim 17$ mM) and high capacity for glucose transport, hence it is most efficient at relatively high glucose concentration [13]. Glut2 is expressed in hepatocytes,

absorptive epithelial cells of the intestinal mucosa and kidney, and pancreatic beta cells. In pancreatic beta cells, by virtue of its low affinity, Glut2 can 'sense' increases in glucose levels and is required for glucose-stimulated insulin secretion [14]. An important consequence of these properties is that Glut2 can adapt its expression and function in response to environmental changes, such as glucose availability in different body compartments. Although this feature might be advantageous during exposure of recirculating T cells to different microenvironments, a putative role of Glut2 in the immune system has not been investigated. In this study, we show that Glut2 is instrumental to the metabolic regulation of effector function in primed CD8+ T cells.

Results

Glut2 regulates CD8+ T cell metabolism.

A putative role of Glut2 in T cell function has not been investigated. As shown in Supplementary Fig. 1 Glut2 is expressed by murine memory T cells as well as other immune cells (Supplementary Fig. 1a-d; panel a shows the gating strategy for flow cytometry, panel c shows confirmation of Glut2 expression on the T cell surface via confocal microscopy). In murine naïve T cells, Glut2 expression was induced by antibody-activation (Supplementary Fig. 1e), peaking 3-4 days after stimulation. Glut1 expression was also increased, peaking 7 days post activation (Supplementary Fig. 1e).

Given its biological function as glucose transporter, the ability of Glut2 to mediate glucose uptake and T cell metabolic reprogramming upon stimulation was investigated by using Glut2 deficient (Glut2-) T cells (Supplementary Fig. 1g) [15].

Uptake of the fluorescent glucose analogue 6-NBDG was significantly reduced in ex vivo Glut2- memory, and in vitro activated CD8+ but not CD4+ T cells (Fig.1a-b). Baseline glucose uptake by either naïve CD4+ or CD8+ T cells was not affected by lack of Glut2 expression (Supplementary Fig. 1h).

We then investigated Glut2-mediated glucose utilization by activated T cells via metabolic fluxometry. As shown in Fig.1c-d, engagement of the glycolytic pathway upon 3-day antibody activation was significantly reduced in Glut2- CD8+ T cells, while it was slightly increased in Glut2- CD4+ T cells. Activated Glut2- CD8+ T cells displayed increased oxidative phosphorylation (OxPhos) (Fig. 1e), possibly as a compensatory response to the reduced energy supply, while mitochondrial respiration was similar in CD4+ T cells irrespectively of Glut2 expression (Fig. 1f). In parallel experiments, we used the Glut1-selective inhibitor STF-31 and the dual Glut1 and Glut2 inhibitor Phloretin[16] to address the relative contribution of these transporters to the glycolytic flux in activated WT CD4+ and CD8+ T cells. Both CD8+

and CD4+ T cells exposed to STF-31 displayed a significantly reduced glycolytic activity, and this effect was more pronounced in the CD4+ subset (Supplementary Fig. 1i-j). Exposure to Phloretin dramatically reduced the glycolytic flux in both CD4+ and CD8+ T cells. These data suggest that both glucose transporters are required to sustain glucose metabolism in CD4+ and CD8+ T cells. Glut1 is instrumental to CD4+ glucose metabolism, this transporter is at least in part redundant in CD8+ T cells. However, in the absence of Glut2 expression, Glut1 contributes to sustaining CD8+ T cell glycolytic activity but the substantial effects of Glut2 deficiency in CD8+ T cells indicate a non-redundant role of this transporter in this subset.

Based on these observations, we used $_{13}C_6$-glucose labeling to study metabolic fluxes in activated Glut2+ and Glut2- $CD8^+$ T cells. As shown in Fig. 1g induction of glycolysis was severely impaired in Glut2- $CD8^+$ T cells as indicated by decreased pyruvate labeling. Although the total level of lactate did not change, the fraction of lactate labelled from glucose was significantly lower compared to that of Glut2+ T cells.

Glut2- $CD8^+$ T cells also displayed a more active TCA cycle as suggested by the presence of more metabolites. However, the fraction of TCA metabolites labelled from glucose was reduced compared to that observed in Glut2+ T cells, suggesting that the increase of these metabolites in Glut2- T cells was from a source different than $_{13}C_6$-glucose.

We also detected an increase in glutamine and glutamate accompanied by a decrease in glutathione (GSH) in Glut2-deficient T cells. The observed increase in both total level and unlabeled fractions might indicate increased glutamine uptake and a decreased synthesis of these metabolites from glucose. In support of this hypothesis, addition of glutamine in the Seahorse base medium increased the glycolytic rate of Glut2- CD8+ T cells to the same levels of Glut2+ CD8+ T cells (Fig 1j).

Thus, increased glutamine uptake and glutamate generation might account for the increase of TCA metabolites, including alpha-ketogluterate (α-KG) and enhanced OxPhos in Glut2- T cells. This compensation might come at the cost of reduced GSH production.

We then analyzed the expression of genes encoding metabolic enzymes by activated Glut2-deficient T cells. Glut2- CD8+ T cells upregulated several genes involved in the glycolytic pathway (Fig. 1k). Amongst the genes encoding enzymes involved in the TCA cycle, Glut2- CD8+ T cells only increased expression of *α-ketoglutarate Dehydrogenase*, in line with the possibility that Glutamine might feed into the TCA cycle in these T cells. In addition, transcription of the gene encoding CPT1a, an enzyme essential for the transport of fatty in the mitochondria, was also significantly upregulated.

Compared to their CD8+ counterpart, Glut2- CD4+ T cells also upregulated transcription of several genes encoding glycolytic enzymes and CPT1a (Supplementary Fig. 1k). In addition, transcription of a larger number of TCA enzyme-encoding genes was significantly increased in Glut2- CD4+ T cells compared to their CD8+ counterpart.

These data indicate that both Glut2- CD8+ and CD4+ T cells undergo a compensatory transcriptional programme capable to correct metabolic pathways only in the CD4+ T cell subset. The lack of TCA gene upregulation – except *α-ketoglutarate Dehydrogenase* - by Glut2- CD8+ T cells might reflect a switch to Glutamine utilization.

Figure 1

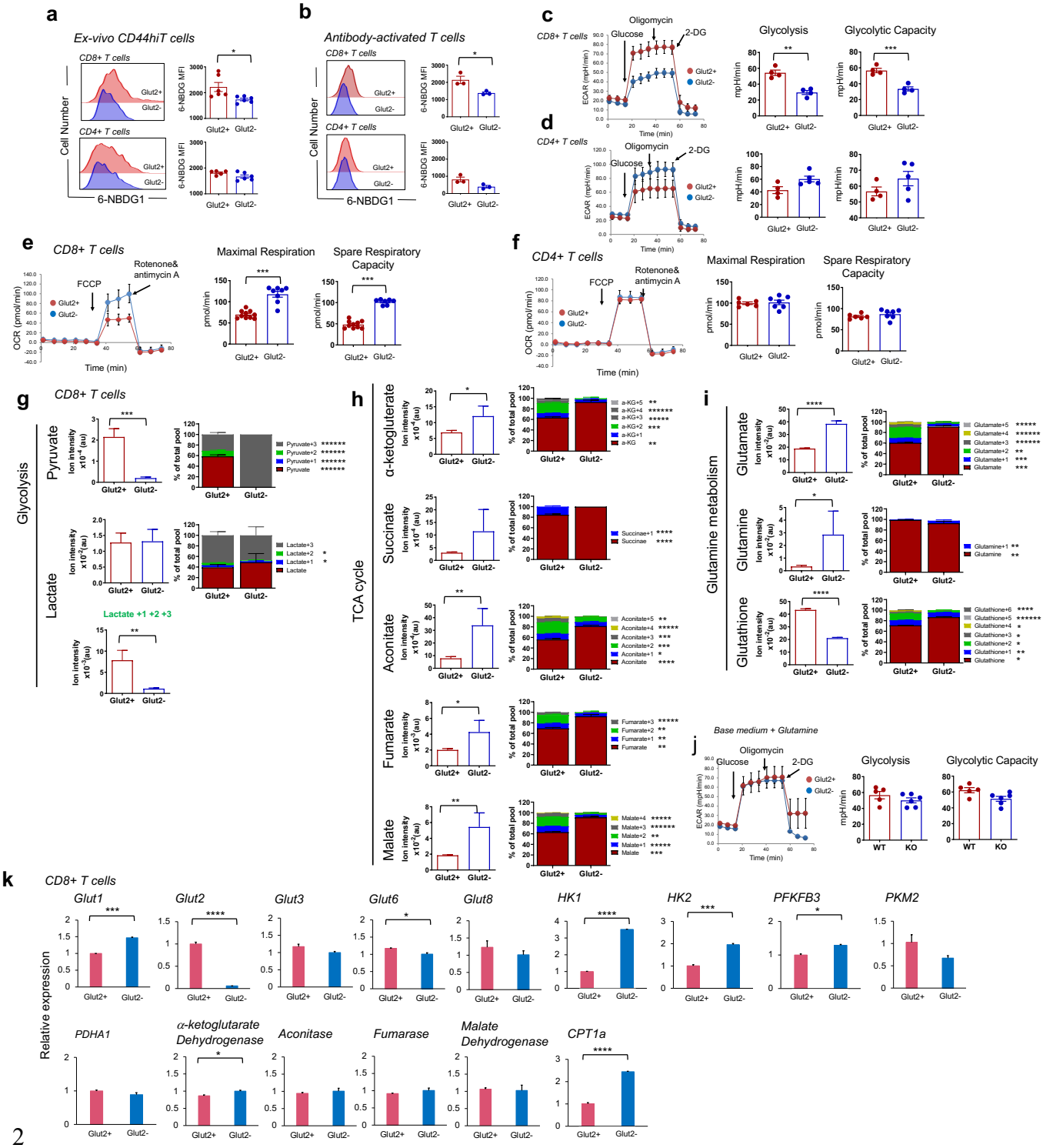

Glut2 affects T cell metabolism.

(**a-b**) 6-NBDG uptake by ex vivo CD44high (**a**) and 3-day *in vitro* activated (**b**) Glut2+ and Glut2- CD8+ and CD4+ T cells was analyzed by flow cytometry. Representative histograms and mean data from 3 independent experiments (±SD; n=3-6) are shown. Unpaired *t*-test.

(**c-d**) Extracellular acidification rate (ECAR, mpH/min) in 2-day activated Glut2+ and Glut2- CD8+ (**c**) and CD4+ (**d**) T cells. The bar graph shows the mean glycolysis and glycolytic capacity (±SD, n=3-5). Unpaired *t*-test.

(**e-f**) Oxygen consumption rate (OCR; pmol/min) in 2-day activated Glut2+ and Glut2- CD8+ (**e**) and CD4+ (**f**) T cells. The bar graph shows the mean maximal respiration and spare respiratory capacity (±SD; n=5-8). Unpaired *t*-test.

(**g-i**): 48 hours activated Glut2+ and Glut2- CD8 T-cells were incubated with $_{13}C_6$-Glucose for 18 hours, followed by metabolites extraction for LC-MS analysis.

Fractional enrichment of glycolysis (**g**), TCA cycle (**h**), and glutamine metabolism (**i**) related $_{13}$C-isotopologues. Columns graphs show total levels of each metabolite in the samples on the left-hand side and the proportion of isotopologues of each metabolite indicated by the 'M+*n*' which designates the position in the molecule where the $_{13}$C label is found on the right-hand side. Data are presented as mean +/- SD. Two-tailed Student's T-test left columns, or Mann–Whitney test, right columns.

(**j**) ECAR (mpH/min) in 2-day activated Glut2+ and Glut2- CD8+ T cells supplemented with glutamine (2mM). The bar graph shows the mean glycolysis and glycolytic capacity (±SD, n=5-6). Unpaired *t*-test.

(**k**) Transcription of the indicated genes in 2-day activated Glut2+ and Glut2- CD8+ T cells was measured by RT-PCR. Gene expression was normalized to housekeeping gene and control Glut2+ set as 1. Error bars show the geometric mean. Kruskal-Wallis test.

*p<0.05, **p<0.01, ***p<0.001, ****p<0.0001, *****p<0.00005, ******p<0.0001

Glut2 regulates CD8+ T cell function.

To explore the physiological relevance of Glut2 expression by T cells, we generated Glut2+ or Glut2- bone marrow (BM) chimeras. A full characterization of Glut2-deficient T cells from these mice is provided in Supplementary Fig. 2.

Proliferation of antibody-stimulated naïve Glut2- T cells was impaired particularly in the CD8+ subset (Fig. 2a). Further, differentiation of Glut2- T cells into the effector memory subset (Tem) both ex-vivo (Supplementary Fig. 2c) and after stimulation in vitro (Supplementary Fig. 2d) was reduced, while no other significant differences were observed.

Glut2+ and Glut2- chimeric mice were primed and boosted 7 days later with ovalbumin plus Poly(I:C) adjuvant by intra-peritoneal (IP) injection, or adjuvant alone as a control. A week after booster immunization, T cells were separately harvested from draining lymph nodes (dLN, mesenteric), non-draining LNs (ndLN, inguinal and axillary) and the spleen. Production of IFN-γ, IL-17 and Granzyme B by CD44high T cells and expression of FoxP3 was assessed by flow cytometry. Production of IFN-γ by Glut2- CD8+ but not CD4+ T cells was reduced (Fig. 2b-c) compared to their Glut2+ counterparts. It is well established that efficient engagement of the glycolytic pathway promotes IFN-γ production via post-transcriptional and epigenetic mechanisms in T cells [17, 18]. To confirm that loss of Glut2 expression led to a decrease of IFN-γ by cell-intrinsic mechanisms, Glut2+ and Glut2- CD8+ T cells were activated in Tc1-polarizing conditions. As shown in Fig. 2d, Tc1-induced and even non-polarized (Tc-0) Glut2- CD8+ T cells displayed a significant defect in IFN-γ production. In addition, production of Granzyme B and expression of the degranulation marker CD107α were significantly decreased in Glut2- CD8+ T cells (Fig. 2e-f). No difference was observed in the expression of IL-17 and FoxP3 (Supplementary Fig. 3a-b).

Together with the overall effect on metabolism, these observations led us to focus on the effector function of Glut2- CD8+ T cells by grafting MHC class I molecule-mismatched B6.Kd [19] skin onto Glut2+ and Glut2- chimeric mice. As shown in Fig. 3a, B6.Kd skin rejection was

significantly delayed in Glut2- BM chimeras. When some of the recipients underwent antibody mediated CD8+ T cell depletion prior to grafting, this resulted in similar rejection kinetics in Glut2+ and Glut2- mice (Fig.3b), further supporting a prominent role of Glut2 in CD8+ T cell effector response.

To determine the effect of Glut2 deficiency on antigen presenting cells, male H-Y antigen-specific TCR-transgenic CD4+ (Marilyn) and CD8+ (Mata Hari) T cells [20, 21] were labelled with CFSE (5μM) and adoptively transferred into Glut2+ and Glut2- female recipients. Twenty-four hours later, recipient mice received male splenocytes intraperitoneally. Five days after immunization, T cells were separately harvested from dLN, ndLN and the spleen, and TCR-transgenic T cell proliferation was assessed. Both male-specific CD4+ and CD8+ T cells proliferated equally well in either Glut-2-competent or -deficient recipients (Supplementary Fig. 3c-d).

Given that lack Glut2 expression appears to severely impair CD8+ T cell effector function, its contribution to anti-tumour immunity was also investigated. As a model, we used orthotopic implantation of the tumor line EO771 (derived from spontaneous breast cancer of C57BL/6 mice) whose growth is efficiently controlled by CD8+ T cells[22], in Glut2+ and Glut2- BM chimeras. Tumor growth was monitored for 28 days (the limit allowed by our Home Office License). At this time point, the tumor volume did not significantly differ between recipients (Fig. 3c). However, when the tumor tissue was analysed, significantly larger areas of necrosis accompanied by reduced tumor-infiltrating lymphocytes (TILs), both indicators of tumor progression, were observed in the Glut2- recipients (Fig 3d-f). Immunofluorescence staining revealed a small but significant decrease of CD4+ T cell infiltration, which was substantial in the CD8+ subset (Fig 3g-i). Expression Glut2 and Glut1 in T cells from splenocytes and TILs from WT BM chimeras were analysed by flow cytometry. As shown in Fig. 3 j-k, Glut 2 expression was significantly decreased in CD8+ but not CD4+ TILs. Conversely, Glut1 expression was significantly increased in CD4+ but not CD8+ TILs. Collectively these data confirm that Glut-2 deficiency impair CD8+ T cell effector function and suggest that expression

of Glut1 and Glut2 are differentially regulated by environmental factors in CD4+ and CD8+ T cells.

Figure 2

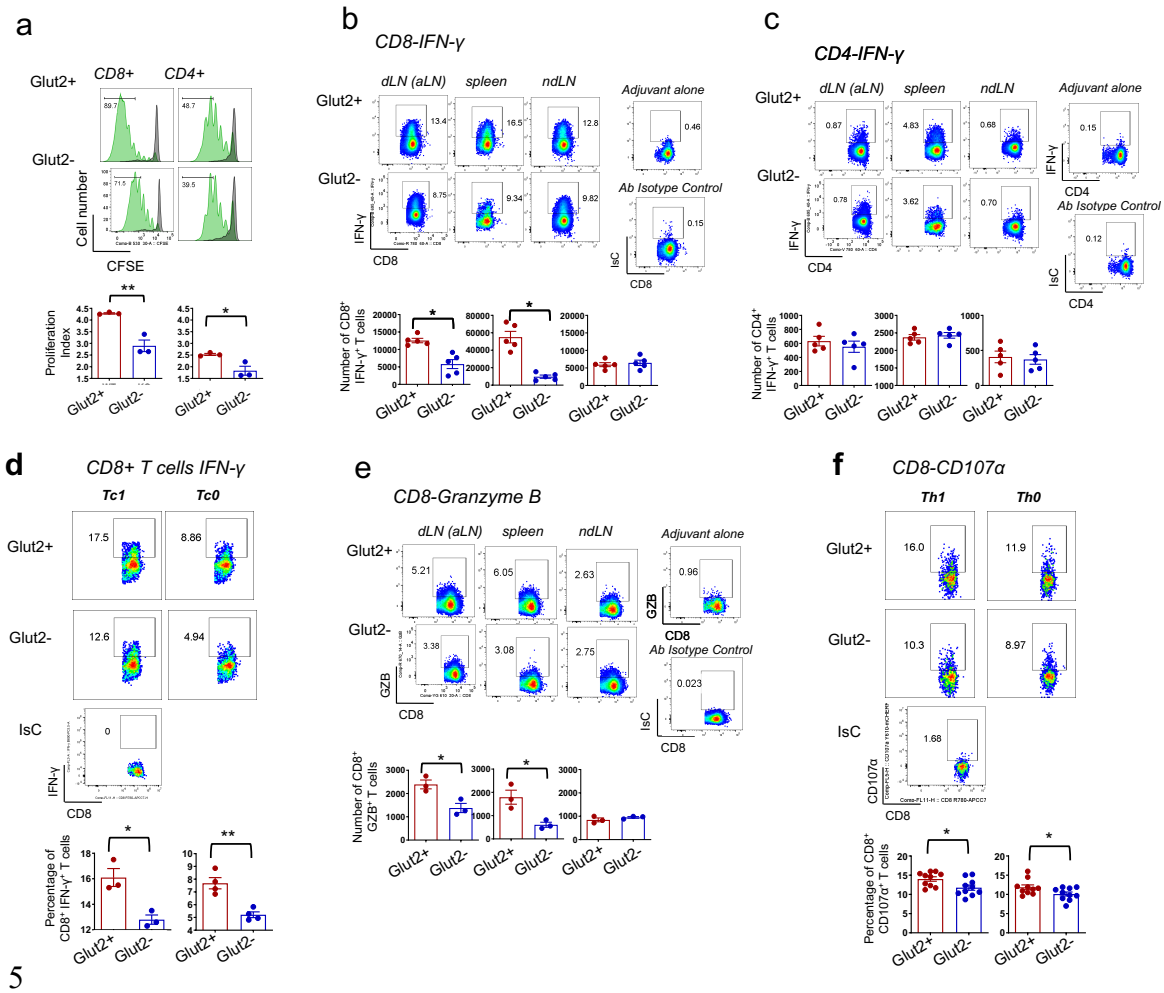

Glut2 contributes to CD8+ T cell function.

(**a**) Naïve Glut2+ and Glut2- CD8+ and CD4+ T cells were labeled with CFSE (5 µM) and stimulated with plate-bound anti-CD3 (1µg/ml) and anti-CD28 (5µg/ml) monoclonal antibodies for 3 days. Proliferation was assessed by flow cytometry. Histograms (grey: unstimulated cells) and mean data from a representative experiment (n=3, N=2) ±SD are shown. Unpaired *t*-test. (**b-c**) Glut2+ and Glut2- chimera mice were primed and boosted (7 days apart) with intra-peritoneal (IP) injection of 750µg ovalbumin protein plus 50µg Poly(I:C) adjuvant or adjuvant

alone. After 7 days, T cells were separately harvested from mesenteric lymph nodes (draining LN, dLN), inguinal and axillary (non-draining LNs, ndLN) and the spleen. Expression of IFN-γ was assessed by flow cytometry. A set of representative dot plots are shown. Control injection with adjuvant alone and staining with an isotype-matched control antibody are shown on the right-hand side of each set. The mean number of IFN-γ+ from a representative of two independent experiments of identical design (with n=3 mice each) is shown (±SD). Percentages are shown within each panel. Unpaired *t*-test.

(**d**) Production of IFN-γ by Glut2+ and Glut2- CD8+ T cells antibody-activated in Tc-1 or Tc-0 polarizing conditions (see Materials and Methods section) was measured by flow cytometry. Unpaired *t*-test.

(**e**) Production of granzyme B by primed (see Panel b) Glut2+ and Glut2- CD8+ T cells from a representative of two independent experiments of identical design (with n=3 mice each) is shown (±SD). Percentages are shown within each panel. Unpaired *t*-test.

(**f**) T cells from Glut2+ and Glut2-deficient mice were activated by plate-bound CD3/CD28 Abs, and differentiated toward Th0, Th1. CD107α was assessed by flow cytometry. A set of representative dot plots and histograms are shown. Unpaired t-test.

*p<0.05, **p<0.01

Figure 3

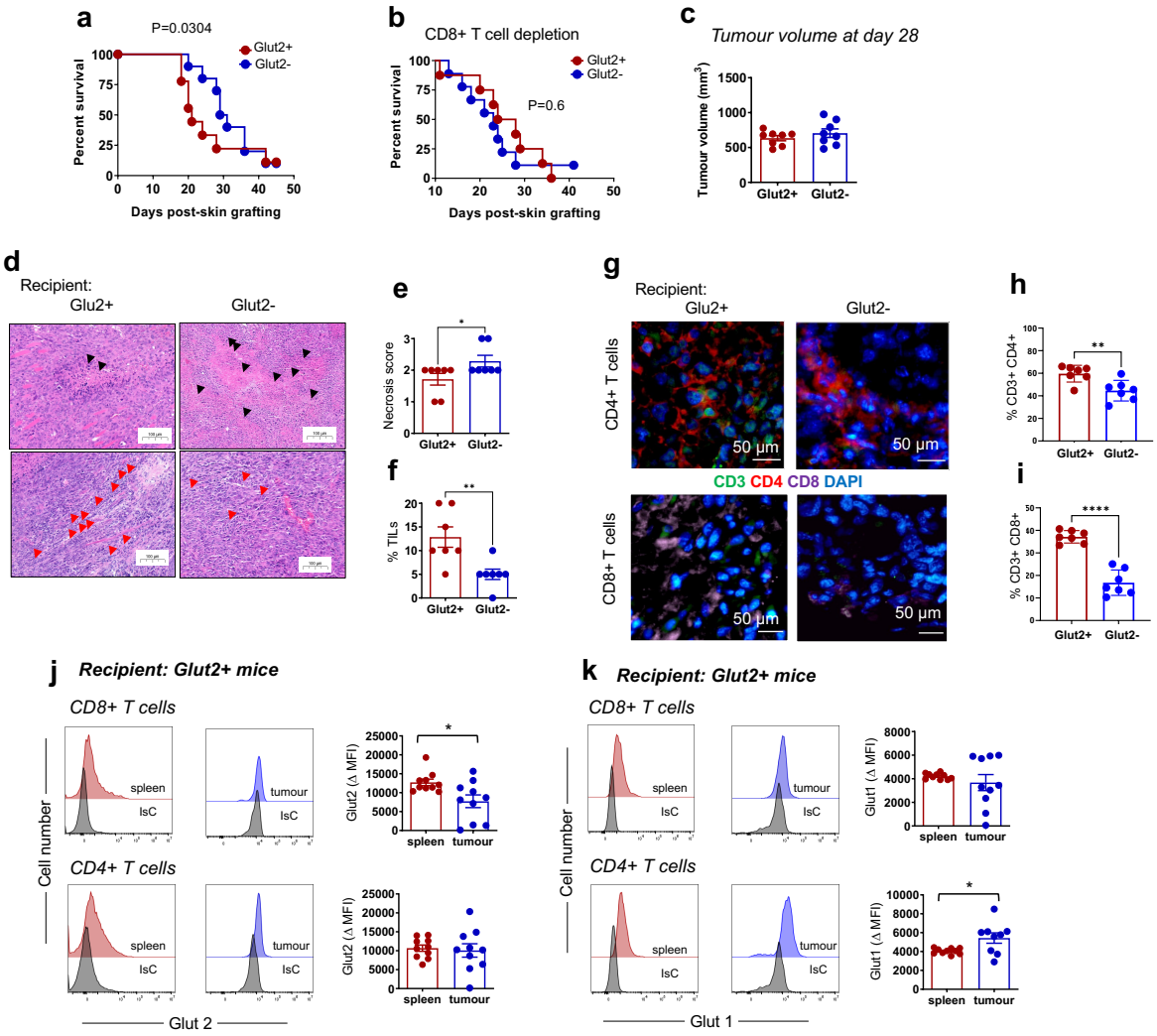

Glut 2 is required for optimal CD8+ T cell-mediated anti-allograft and anti-tumour immunity.

(**a-b**) Glut2+ or Glut2- mice received skin graft from B6.Kd donors. CD8+ T cell depletion was achieved by IP injection of 200 µg anti-CD8 at days –1 and 1 (**b**). Log-rank (Mantel-Cox) test. P values of the mean time of rejection are indicated within the graphs (n=8-10).

(**c**) EO771 cells were injected into of the mammary glands of female Glut2+ or Glut2- C57BL/6 mice (n = 10). The values of tumor volume (mm3) are reported (mean ± SD).

(**d, e, f**) Tumor tissue were embedded in paraffin for H&E staining for assessment of necrosis (**e**) and the percentage of tumor-infiltrating lymphocytes (**f**). Unpaired t-test.

(**g, h, i**) Immunofluorescence staining of CD3, CD4, CD8 , and DAPI in OCT-embedded tumour sections was analysed and quantified for % of CD3+CD4+ T cells (**h**), and %CD3+CD8+ T cells (**i**). Unpaired t-test.

(**j, k**) T cells from tumor and spleen were assessed for surface expression of glut2 (**j**) and glut1 (**k**) by flow cytometry. Delta changes of Mean Florescence Intensity (MFI) in glut2 and glut1 were determined by subtraction of isotype control from antibody staining. Unpaired t-test.

*p<0.05, **p<0.01, ****p<0.0001

Glut2 expression by T cells is modulated by glucose, extracellular pH and oxygen availability.

In pancreatic beta cells, Glut2 expression is regulated by microenvironmental changes [23]. As memory T cells recirculate through vascular and tissue sites where glucose availability, acidification and oxygen tension differ, such as blood, lymphoid tissue and inflammatory sites, the relative effect of these environmental components on Glut2 expression and function were investigated.

We first assessed the effect of glucose availability on Glut2 expression. As shown in Fig. 4a-b, activation-induced increase of Glut2 and Glut1 expression by CD8+ and CD4+ T cells was significantly blunted by glucose concentrations above 5mM.

To evaluate the effect of extracellular acidification on Glut2 expression, T cells were antibody-activated in medium at pH 7.4 or pH 6.3. As shown in Fig. 4c-e, a decrease in pH led to a substantial reduction in the expression of both Glut2 and Glut1 and 6NBDG uptake by both CD8+ and CD4+ T cells.

Finally, to measure the effect of oxygen availability on Glut2 expression, T cells were antibody-activated for 2 days and subsequently maintained in high (20%) or low (5%) oxygen concentrations for the last 24 hours of culture [24]. As shown in Fig. 4f, Glut2 expression by CD8+ T cells was significantly reduced in hypoxic conditions. Glut2 expression by CD4+ T cells did not change in different oxygen concentrations. Conversely, Glut1 expression was upregulated by CD4+ and only marginally by CD8+ T cells at 5% oxygen (Fig 4g). Accordingly, 6-NBDG uptake by CD8+ T cells was increased in high oxygen cultures, while CD4+ T cells enhanced 6-NBDG uptake in low oxygen conditions (Fig. 4h).

Overall, these data show that expression of both Glut1 and Glut2 by T cells is dictated by environmental cues and is regulated by glucose concentration and extracellular acidification in the same manner. However, Glut2 expression is directly proportional to oxygen availability in CD8+ T cells, while a decrease in oxygen leads to an increase in Glut1 expression in both

CD4+ and CD8+ T cells, suggesting a different regulation of these two transporters by oxygen levels.

Figure 4

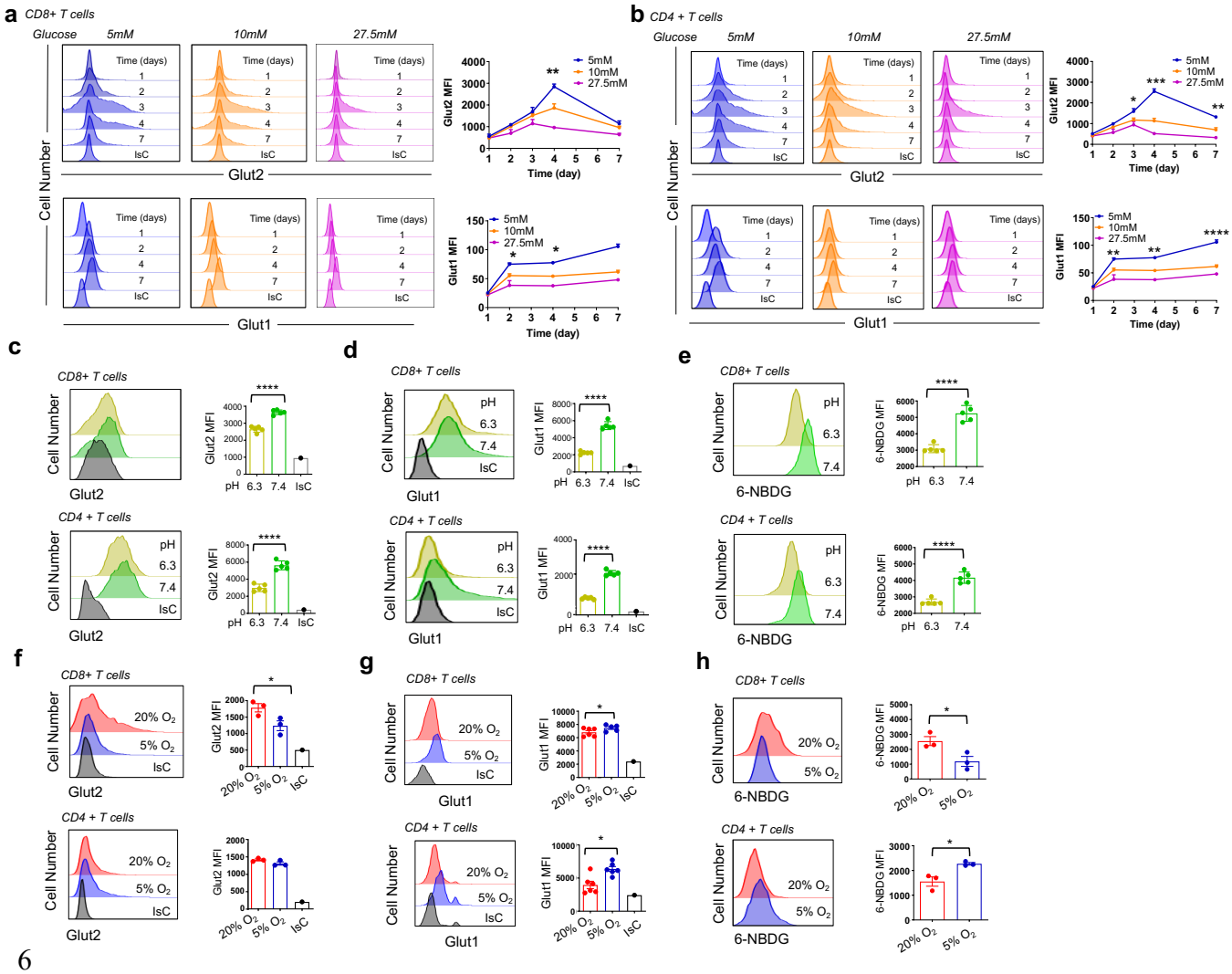

Regulation of Glut expression by environmental factors

(**a-b**) Murine naïve T cells were antibody-activated in medium containing different concentrations of glucose for 7 days before assessing surface Glut2 and Glut1 expression by by CD8+ (**a**) and CD4+ (**b**) T cells by flow cytometry. Histograms and mean data (±SD) from a representative experiment (n=3, N=3) are shown. One-way ANOVA.

(**c-e**) T cells were antibody-activated in medium with either pH 6.3 or 7.4 for 3 days before analyzing surface expression of Glut2 (**c**), Glut1 (**d**), and 6-NBDG uptake (**e**) by flow cytometry. Histograms and mean data (±SD) from a representative experiment (n=3, N=3) are shown. Unpaired *t*-test.

(**f-k**) Naïve T cells were antibody-activated for 2 days and subsequently maintained in high (20%) or low (5%) oxygen concentrations for the last 24 hours of culture. Surface expression of Glut2 (**f**), Glut1 (**g**), and 6-NBDG uptake (**h**) was then analyzed by flow cytometry. Histograms and mean data (±SD) from a representative experiment (n=3, N=3) are shown. Unpaired *t*-test.

*p<0.05, **p<0.01, ***p<0.001, ****p<0.0001

Glut2 expression by CD8+ T cells is indirectly regulated by HIF1α via Galectin-9.

The observation that oxygen availability modulates Glut2 expression by T cells is consistent with a potential mechanistic role for the oxygen sensor hypoxia-inducible factor (HIF)1α. We confirmed that HIF1α is stabilized and translocates to the T cell nucleus at 5% oxygen concentration used in the experiments above (Supplementary Fig. 4a-b). The gene encoding Glut1 is positively regulated by HIF1α [25], while HIF1α activation has been reported to reduce Glut2 expression in muscle [26]. We therefore investigated the effect of HIF1α pharmacological and genetic inactivation on Glut2 and Glut1 expression. As shown in Fig. 5a-c, Glut2 expression by CD8+ T cells was significantly enhanced by exposure to a selective HIF1α inhibitor, PX-478 [27] both *in vitro* (Fig. 5a) and *in vivo* (Fig. 5c). As expected, expression of Glut1 was reduced by exposure to the inhibitor (Fig. 5b).

We confirmed these observations by analyzing Glut2 and Glut1 expression by T cells from *CD4*^{Cre}*HIF1α*^{flox,flox} (HIF-) mice, in which also CD8+ T-cells lack HIF1α gene expression (Supplementary Fig. 4c) probably due to 'leakage' during thymic development. As shown in Fig. 5d, antibody-activated CD8+ T cells from HIF- mice displayed increased expression of Glut2 compared with those from *HIF1α*^{flox,flox} (HIF+) control mice.

Surprisingly, while Glut1 transcription was decreased in HIF- CD8+ T cells (Fig. 5e), transcription of Glut2 was not affected by HIF1α deficiency (Fig. 5f), suggesting that post-transcriptional mechanisms are responsible for HIF1α-mediated modulation of Glut2 expression.

Glut2 is a N-glycosylated glycoprotein, whose residency on the surface of pancreatic beta cells is maintained by binding to the lectin Galectin-9 (Gal-9) via its N-glycan branches [28]. Gal-9 is a glycan-binding protein secreted by many cells, and is known to regulate the effector and regulatory phases of the immune response, by inhibiting Th1 cell responses via binding to Tim-3 [29, 30], and by promoting the generation of inducible regulatory T cells through interactions with CD44 [31].

HIF1α has been shown to upregulate Gal-9 expression [32]. Accordingly, Gal-9 gene and protein expression was significantly reduced in CD8+ T cells from HIF- mice (Fig. 5g-h). Consistently, Gal-9 expression was increased in CD8+ T cells activated in low compared to high oxygen concentrations (Fig. 5i). Glut2 expression by antibody-activated Gal-9-deficient (Gal-9-) CD8+ T cells was significantly higher compared to that of their Gal-9+ counterpart (Fig. 5j). Vice-versa, addition of recombinant Gal-9 decreased Glut2 expression by activated WT CD8+ T cells, and this was reversed by addition of the Gal-9 competitive inhibitor, lactose (Fig. 5k) [33]. A possible role for the HIF/Gal-9 axis in the regulation of Glut2 expression by activated CD4+ T cells was also investigated. As shown in Supplementary Fig. 4d-e, Glut2 and Gal-9 expression levels were only mildly increased in HIF- activated CD4+ T cells. In addition, Gal-9- activated CD4+ T cells did not display increased Glut2 expression (Supplementary Fig. 4f). Interestingly, addition of recombinant Gal-9 to antibody-activated CD4+ T cells led to decreased Glut2 expression (Supplementary Fig. 4g), raising the possibility that CD4+ T cells might not produce levels of Gal-9 sufficient to downregulate Glut2 expression. Consistently, we observed that surface expression of Gal-9 is significantly lower in CD4+ T cells compared to CD8+ T cells (Supplementary Fig. 4h).

We further measured the metabolic features of Gal-9- CD8+ T cells (Fig.5l-m), which, as expected, displayed significantly enhanced glycolysis with no changes in the OxPhos rate.

Finally, we generated Gal-9+ and Gal-9- BM chimeras, which received skin grafts from MHC class I-mismatched B6.Kd donors. Rejection of B6.Kd skin grafts by Gal-9- recipients was accelerated compared with that by Gal-9+ chimeras (Fig. 5n). To further confirm the prominent role of Gal-9 expression by CD8+ T cells, donor B6.Kd skin was grafted onto CD8+ T cell-depleted Gal-9+ or Gal-9- chimera recipients. Removal of CD8+ T cells led to similar graft rejection kinetics by both recipients (Fig. 5o).

Figure 5

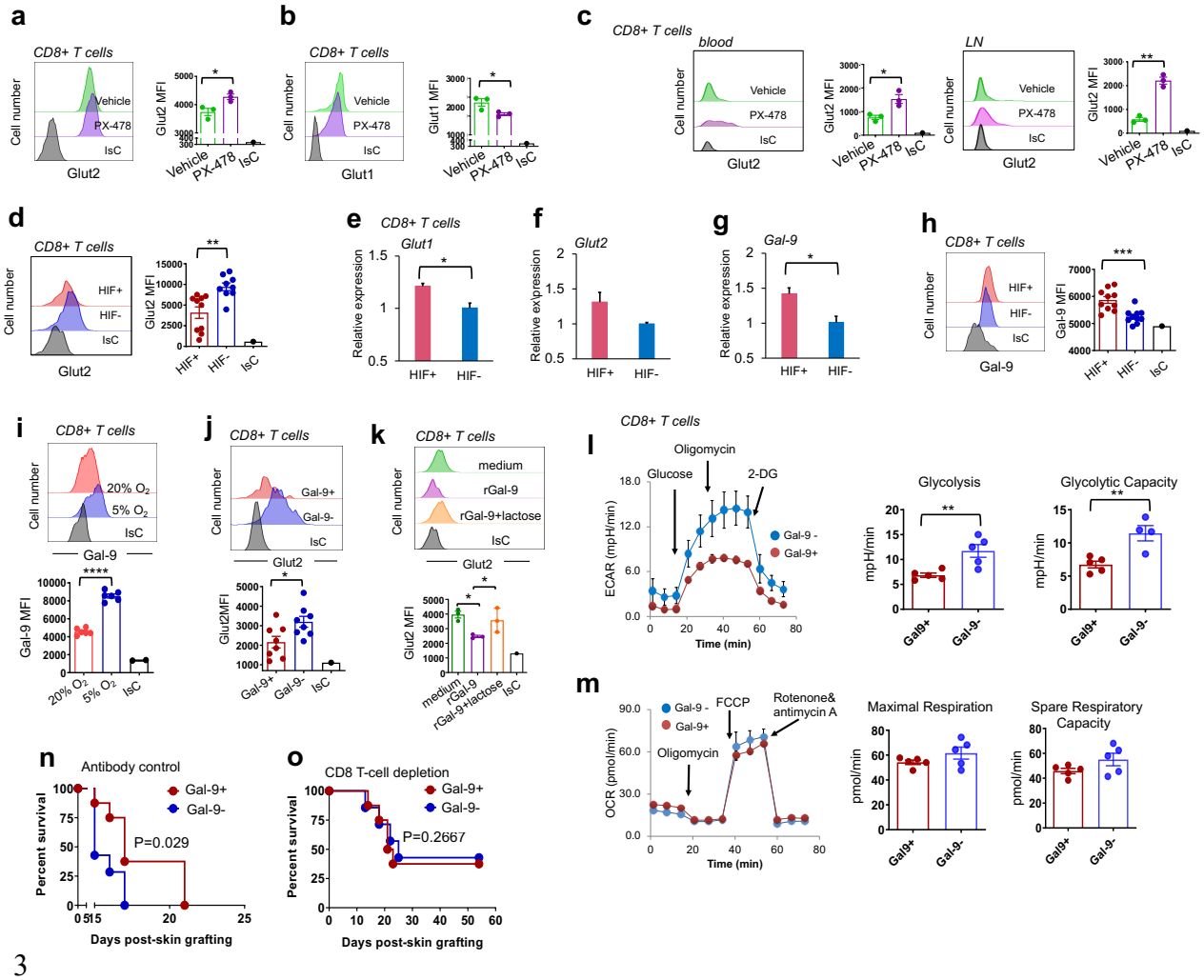

Regulation of Glut2 expression by HIF1α and Galectin-9.

(**a-b**) Murine naïve CD8+ T cells were antibody-activated in the presence or absence of the HIF1α selective inhibitor PX-478 (20μM) before analyzing surface expression of Glut2 (**a**) and Glut1 (**b**) by flow cytometry. Histograms and mean data (±SD) from a representative experiment (n=3, N=3) are shown. Unpaired *t*-test.

(**c**) C57BL/6 mice received an IP injection of PX-478 (20mg/kg) for 3 consecutive days. CD8+ T cells were separately harvested from blood and LN for assessment of surface Glut2 expression. Representative histograms and mean data (±SD) from a representative experiment (n=3, N=2). Unpaired *t*-test.

(**d**) Expression of Glut2 by CD44high CD8+ T cells from HIF+ or HIF- mice was assessed by flow cytometry. Histograms and mean data from 3 independent experiments are shown (±SD). (N=3, n=3) Unpaired *t*-test.

(**e-g**) Transcription of Glut1 (**e**), Glut2 (**f**) and Gal-9 (**g**) by CD44high CD8+ T cells from HIF+ and HIF- mice was measured by RT-PCR. Gene expression was normalized to the housekeeping gene tubulin. Control HIF- was set as 1. Error bars show the geometric mean. (N=3) Kruskal-Wallis test.

(**h**) Spleen CD8+ T cells from HIF+ and HIF- mice were assessed for surface expression of galectin-9 (Gal-9) by flow cytometry. Histograms and mean data (±SD) from a representative of 3 experiment are shown. (N=3 n=3) Unpaired *t*-test.

(**i**) Spleen naïve CD8+ T T cells were antibody-activated for 2 days and subsequently maintained in high (20%) or low (5%) oxygen incubators for the last 24 hours of culture. Gal-9 surface expression was then measured by flow cytometry. Histograms and mean data (±SD) from a representative experiment are shown (N=3 n=3). Unpaired *t*-test.

(**j**) Glut2 expression by CD44high T cells from Gal-9+ or Gal-9- mice was assessed by flow cytometry. Histograms and mean data (±SD) from a representative experiment are shown. (N=3 n=3) Unpaired *t*-test.

(**k**) Spleen naïve T cells were antibody-activated in the presence or absence of recombinant Gal-9 (30nM) with or without the Gal-9 competitive inhibitor lactose (30mM) before analyzing surface expression of Glut2 by flow cytometry. Histograms and mean data (±SD) from a representative experiment. (N=3 n=3) One-way ANOVA.

(**l-m**) Murine CD8+ T cells were isolated from Gal-9+ and Gal-9- mice and antibody-activated for 2 days. Extracellular acidification rate (ECAR, mpH/min) in 2-day activated CD8+ T cells (**l**). The bar graph shows the mean glycolysis and glycolytic capacity (±SD, n=5). Oxygen consumption rate (OCR; pmol/min) in 2-day activated CD8+ T cells (**m**). The bar graph shows the mean maximal respiration and spare respiratory capacity (±SD; n=5). Unpaired *t*-test.

(**n-o**) Gal-9+ and Gal-9- mice received skin grafts from BL/6.Kd donors (**n**). CD8+ T cell depletion was achieved by IP injection of 200 μg anti-CD8 at days –1 and +1 (o). Log-rank (Mantel-Cox) test. P values of the mean time of rejection are indicated within the graphs (n=6-8).

*p<0.05, **p<0.01, ***p<0.001, ****p<0.0001

Stomatin stabilizes surface expression of Glut2 by CD8+ T cells.

Membrane sub-domain distribution of Glut2 is associated with the glucose transport activity of pancreatic beta cells, in which binding to Gal-9 maintains Glut2 location in non-lipid raft domains [34]. This effect is counteracted by Stomatin, which is a lipid raft-residing protein. In beta cells, Stomatin directly binds to the cytosolic C-terminal tail of Glut2, provoking its relocation to lipid rafts [34].

In T cells, up-regulation of Stomatin expression and its coalescence to the immunological synapse during activation increases effector responses, while down-regulation of stomatin expression correlates with loss of sustained TCR signalling and decreased T cell activation [28]. We therefore investigated a putative role of Stomatin in stabilizing the surface expression of Glut2.

Stomatin is upregulated upon antibody activation (Supplementary Fig. 5a) and is expressed on the surface of CD44high T cells in secondary lymphoid organs and in blood - in which it is significantly higher - and its expression is directly proportional to that of Glut2 (Fig. 6a-b). Moreover, Glut2 but not Glut1 upregulation following antibody-activation was significantly blunted by a Stomatin-blocking antibody in CD8+ T cells (Supplementary Fig.5b, Fig. 6c-d).

To understand the mechanistic relationship between Glut2, Gal-9 and Stomatin in CD8+ T cells, we subsequently undertook a series of deconvolution microscopy imaging experiments. First, we monitored co-localization of Gal-9, Stomatin, CD3 and Glut2 by CD8+ T cells before (day 0) and following antibody activation (day 3 and day 5) as previously described [35]. The expression of Stomatin, Gal-9 and Glut2, measured as corrected total cell fluorescence (CTCF), is shown in Supplementary Fig. 5b. As expected, Stomatin co-localized with CD3 by 3 days after activation and remained stable until day 5 (Fig. 6e). In parallel, Stomatin co-localization with Glut 2 was still increasing 5 days after activation (Fig. 6f). In contrast, Gal-9 co-localization with CD3 was maximal 3 days after activation but declined by day 5 (Fig. 6g). Accordingly, Glut2 co-localization with Gal-9 peaked at day 3 and was significantly reduced at day 5 (Fig. 6h).

Second, we obtained evidence of a putative competition mechanism between Stomatin and Gal-9 by showing that addition of exogenous recombinant Gal-9 reduced both expression and co-localization of both Glut2 and Stomatin with CD8 (surrogate for lipid raft segregation; Fig. 6i-j). Overall, these data suggest that membrane redistribution and expression of Glut2 is dynamically orchestrated by interaction with Gal-9 and Stomatin.

Figure 6

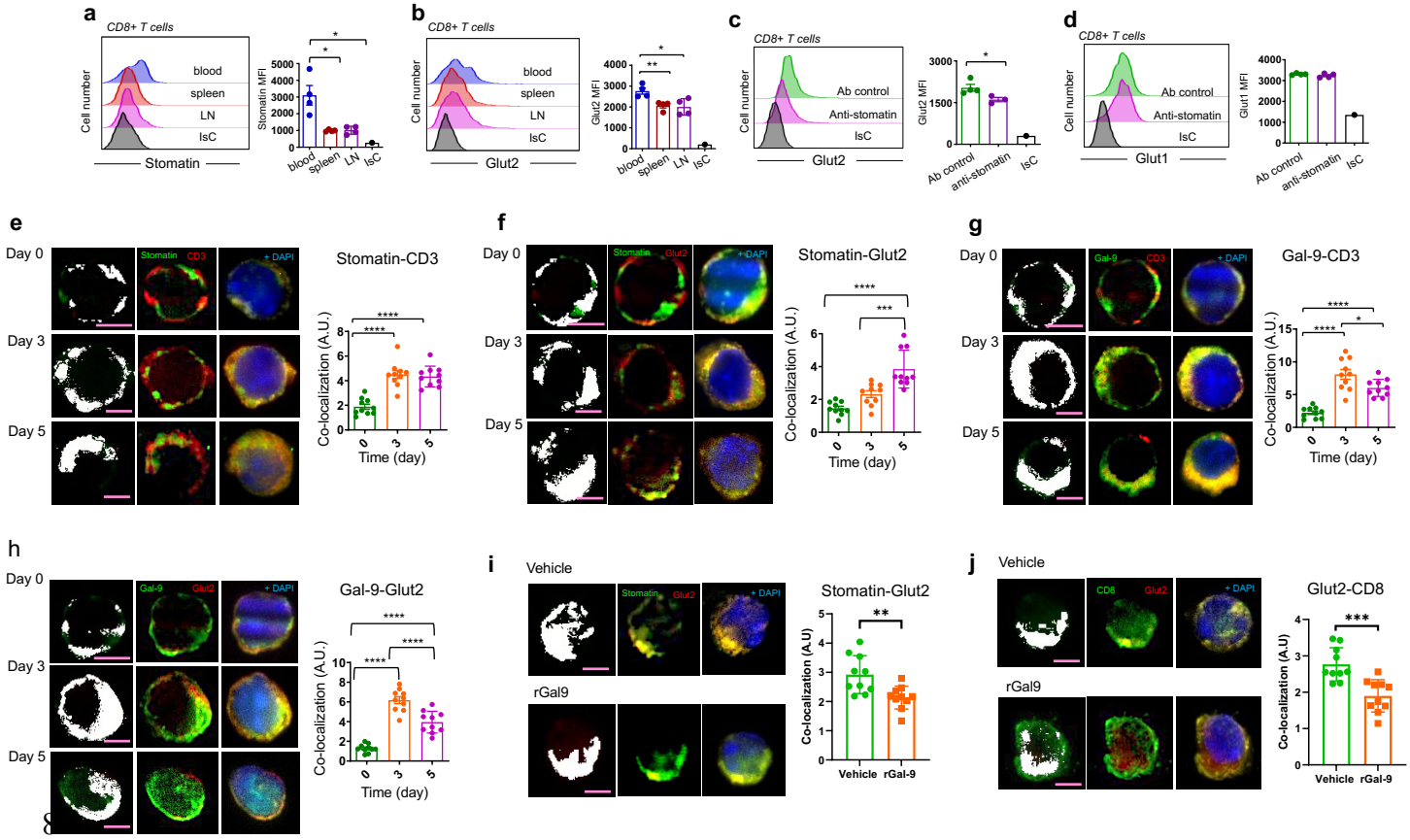

Stomatin and Galectin-9 mediate regulation of Glut2 expression.

(**a-b**) Surface expression of Stomatin (**a**) and Glut2 (**b**) by CD44high CD8+ T cells from blood, spleen, and LN was analyzed for by flow cytometry. Histograms and mean data (±SD) from a representative experiment ±SD (n=3, N=3)**.** One-way ANOVA.

(**c-d**) Naïve CD8+ T cells were antibody-activated in the presence of anti-stomatin or isotype control antibody before analyzing Glut2 (**c**) and Glut1 (**d**) expression by flow cytometry. Histograms and mean data (±SD) from a representative experiment (n=3, N=3). Unpaired t-test.

(**e-h**) Naïve CD8+ T cells were antibody-activated for 3 or 5 days before analyzing surface expression of Glut2, Stomatin, Gal-9, and CD3 by deconvolution microscopy. Representative deconvolution and channel colocalization images of stomatin/CD3 (**e**), stomatin/Glut2 (**f**), Gal-9/CD3 (**g**), and Gal-9/Glut2 (**h**) of non-permeabilized cells at day 0 (naïve) and at day 3 and day 5 after activation are shown. Colocalization of different channels is indicated by the white areas in the cell images and presented as % of cell volume. Bar charts show the mean % of cell volume in at least 10 cells from a representative of 3 experiments. One-way ANOVA.

(**i, j**) Naïve T cells were antibody-activated in the presence or absence of recombinant Gal-9 (30nM) before analyzing surface expression of Glut2, stomatin, and CD8+ by deconvolution microscopy. Representative deconvolution and channel colocalization images of stomatin/Glut2 (**i**) and Glut2/CD8 (**j**) are shown. Colocalization of different channels is indicated by the white areas in the cell images and presented as % of cell volume. Bar charts show the mean % of cell volume in at least 10 cells from a representative of 3 experiments. Unpaired t-test.

*p<0.05, **p<0.01, ***p<0.001, ****p<0.0001

Kinetics of Glut2 expression define its function in CD8+ T cell responses *in vivo*.

We next sought to validate the physiological relevance of Glut2 regulation in distinct phases of the immune response when T cells localize to different microenvironments. To this aim, we used CD8+ HY-specific H2d-restricted TCR-transgenic Mata Hari (MH) T cells. Naïve CD45.2 MH T cells were adoptively transferred into CD45.1 syngeneic female recipients. The next day some mice were immunized IP with male splenocytes and the expression of Glut2 by recirculating CD45.2+ CD44high (primed) CD8+ MH T cells was assessed for the following 5 days. As shown in Fig. 7a, Glut2 expression increased on recirculating primed MH CD8+ T cells, peaking 3-4 days after immunization, while it did not change on recipient memory T cells. Glut1 expression was also upregulated by primed T cells and was still increasing 5 days after immunization (Fig. 7b), as we observed following activation in vitro (Supplementary Fig. 1e-f).

To model a non-lymphoid antigenic site, mice received a further intraperitoneal injection of male splenocytes plus CXCL10 to promote local inflammation 7 days after the initial priming. Glut2 expression by primed MH T cells was assessed after 16 hours to avoid the confounding effect of further antigen-induced T cell division. As shown in Supplementary Fig. 6a-b, primed MH T cell migrated to the peritoneum and spleen, indicating their recirculation out of the lymph nodes and to antigen-rich tissue. No difference was found in the distribution of naïve MH T cells. While maintained in secondary lymphoid organs, Glut2 expression was dramatically reduced in primed T cells migrated to the peritoneum (Fig. 7c). In contrast, Glut1 expression by primed MH T cells did not significantly change (Fig. 7d).

We further investigated the physiological role of Glut2 in glucose uptake by T cells in different tissue environment in vivo. It was technically unfeasible to address this question using the model described above as in our hands 6-NBDG fluorescence becomes undetectable within 60 minutes from injection. Glut2- or Glut2+ chimeras were starved for 2 hours before systemic administration of 6-NBDG at 5mg/kg. Thirty minutes after injection, 6-NBDG uptake by T cells harvested from blood, LN and spleen was assessed by flow cytometry. As shown in Fig. 7e,

6NBDG uptake by Glut2- CD44high CD8+ T cells was severely impaired in blood but unchanged in spleen and lymph nodes. Of note, 6-NBDG uptake in the blood was significantly higher in CD8+ compared with CD4+ Glut2+ T cells, while uptake in lymph nodes and spleen was similar in both subsets (Fig. 7f). No difference in glucose uptake was observed in Glut2+ and Glut2- naïve (CD44low) CD8+ and CD4+ T cells (Supplementary Fig. 6d-e). Overall, these data suggest that, compared to memory CD4+ T cells, primed CD8+ T cells physiologically take up a large amount of glucose while recirculating in the blood in a Glut2dependent manner. In CD8+ lymphocytes, glucose taken up is partially stored as glycogen. CD8+ T cells have been shown to possess the enzymatic machinery for both glycogen synthesis and glycogenolysis [36]. As shown in Fig. 7g and Supplementary Fig. 6f, intracellular glycogen is significantly higher in Glut2+ memory CD8+ T cells compared to CD4+ T cells and glycogen stores are depleted in Glut2- CD8+ but not CD4+ T cells.

On this basis, we took advantage of the reduced ability of HIF-1α-deficient CD8+ T cells to downregulate Glut2 to challenge the hypothesis that the substantial downregulation of Glut2 expression by CD8+ T cells in inflammatory sites might prevent glucose leakage, especially given the inability of these cells to upregulate Glut1. Equal numbers of HIF+ and HIF- naïve CD8+ T cells were antibody-activated for 3 days, labelled with 6-NBDG and injected IP in mice which had received IFN-γ and CXCL10 IP 48 hours earlier to generate an inflammatory environment (Fig. 7h). 6NBDG uptake was measured before and 30 minutes after injection. As expected, glucose uptake by CD8+ HIF- T cells was significantly higher than that of HIF+ CD8+ T cells (Fig. 7i). However, when 6NBDG expression was measured after retrieving the T cells, 6-NBDG content was similar in HIF1+ and HIF1- CD8+ T cells (Fig. 7j). Differential glucose leak was calculated by subtracting 6-NBDG MFI in T cells retrieved in the peritoneum from that displayed before injection and showed a significantly higher loss of 6-NBDG by HIF- T cells (Fig. 7k). A comparison of the peritoneal fluids showed a significantly higher 6-NBDG concentration in recipients of HIF- CD8+ T cells (Supplementary Fig. 6g-h).

Figure 7

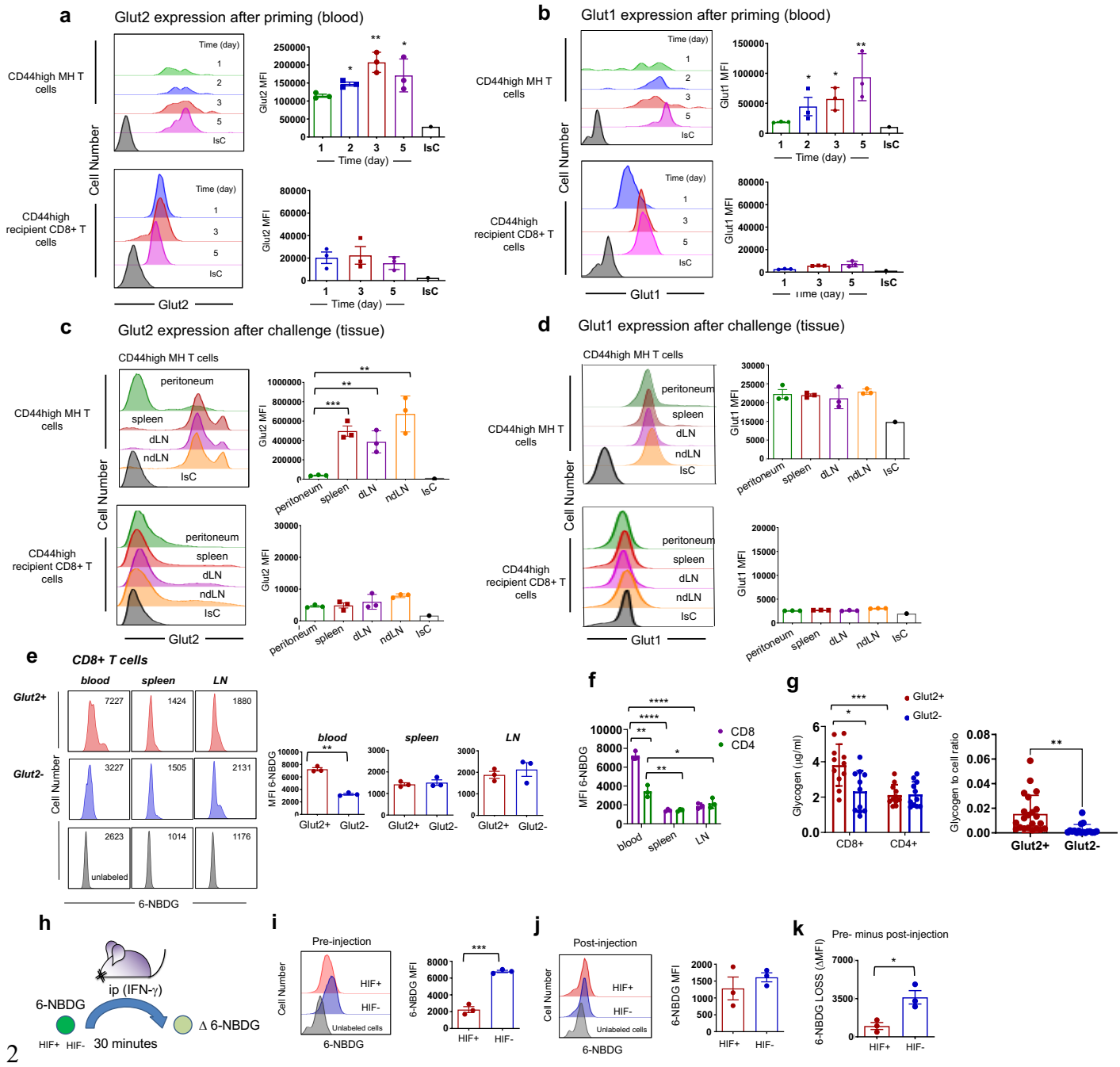

In vivo Glut2 expression and function in T cells

(**a-d**) Purified CD45.2+ Mata Hari CD8+ naïve T cells (MH) were adoptively transferred (10^7) into CD45.1+ recipients, some of which received male splenocytes ($2x10^7$) IP a day later. Tail blood was sampled on the indicated days, and Glut2 (**a**) and Glut1 (**b**) expression by T cells was analyzed by flow cytometry. Recipient CD45.1+ CD44high T cells are shown for

comparison. After 7 days, each mouse received male splenocytes ($20x10^6$) and 1.2 µg CXCL10 IP. T cells were harvested from peritoneum, spleen, mesenteric LN (draining LN, aLN), and axillary LN (non-draining LN, ndLN) 16 hours later. Expression of Glut2 (**c**) and Glut1 (**d**) by CD44hi MH T cells and CD44hi recipient CD8+ T cells was assessed by flow cytometry. A set of representative histograms is shown. The bar graphs show the mean fluorescence intensity (MFI) measured for Glut2 and Glut1 (±SD; n=3) in a representative experiment (N=2). One-way ANOVA.

(**e-f**) Glut2+ or Glut2- mice were starved for 2 hours before IV injection of 6-NBDG (5mg/Kg). 30 minutes later, T cells were harvested from blood, spleen, and LN. 6-NBDG uptake was assessed by flow cytometry. A set of representative histograms are shown. The bar graphs show the mean fluorescence intensity (MFI) of 6-NBDG (**e**). (**f**) Comparison of 6-NBDG uptake in CD8+ and CD4+ T cells from different tissues (±SD; n=3). One-way ANOVA.

(**g**) Glycogen content in 3-day activated Glut2+ and Glut2- naive T cells was measured as described in the methods section. Data were normalized by protein content (±SD; n=1, N=2). On the right-hand side, glycogen to cell ratios measured for images by transmission electron microscope. Unpaired *t*-test.

(**h-j**) CD45.2+ HIF1+ or HIF1- naïve CD8+ T cells were antibody-activated for 3 days, labelled with 6-NBDG and injected IP (10^7) in CD45.1+ mice which had received IFN-γ IP 48 hours previously to induce inflammation (**h**). 6-NBDG uptake by HIF+ and HIF- T cells was measured by flow cytometry before injection (pre-injection, **i**) and in T cells retrieved from the peritoneal lavage 30 minutes after injection (post-injection, **j**). Representative histograms are shown. The bar graphs show the mean fluorescence intensity (MFI) ±SD in 3 independent experiments. Unpaired *t*-test.

(**k**) Loss of incorporated 6-NBDG was calculated by subtracting the 6-NBDG MFI post-injection to the pre-injection values. (n=3, N=2). Unpaired *t*-test.

*p<0.05, **p<0.01, ***p<0.001, ****p<0.0001

Glut2 contributes to human T cell responses.

Inactivating mutations of Glut2 in humans cause Fanconi–Bickel syndrome, a severe paediatric condition characterized by hepatomegaly, growth retardation, renal syndrome, and, notably, associated with recurrent infections particularly of the lower respiratory tract [37, 38].

To assess a potential role of Glut 2 in the human system we analyzed T cells from carriers of a rare polymorphism in the Glut2-encoding SLC2A2 gene (SNPs rs5400 [T110I]). Albeit not severely abrogating glucose uptake by Glut2, T110I has been associated with decreased fasting plasma glucose and insulin [39]. These parameters measured in our study population are shown in Supplementary Table 1.

CD4+ and CD8+ T cells were isolated from peripheral blood mononuclear cells (PBMC) and expression of Glut2 was assessed by Flow cytometry. As shown in Fig. 8a, ex vivo expression of Glut2 in CD4+ and CD8+ T was similar in WT and T110I SNP carriers, irrespectively of the amount of glucose added to the cultures (Fig. 8b). However, 6-NBDG uptake, despite similar after ex vivo incubation (Fig. 8c), was significantly reduced in both T110I CD4+ and CD8+ T cells following antibody-activation, irrespectively of the amount of glucose added to the cultures (Fig. 8d), indicating that Glut2 contributes to glucose uptake in human T cells and that, unlike in murine T cells, glucose concentrations do not affect its expression and function.

When T cell differentiation was analyzed, we observed a significant decrease in the proportion of TEMRA (CD45RA+, CCR7-) CD8+ T cells in T110I SNP carriers which was accompanied by an increase of T cells with an effector memory phenotype (Fig. 8e-h). This is in line with the observation made in Glut2-deficient murine T cells, which displayed significantly reduced terminal differentiation both in vitro and in vivo (Supplementary Fig. 2c-d) (bearing in mind that a TEMRA phenotype has not been described in mice [40]).

We did not detect differences between WT and T110I carriers in terms of T cell proliferation and IFN-γ production (Supplementary Fig. 7a-c and d-e, respectively).

Given the limitations imposed by the relatively small number of T110I SNP carriers and the mild effect of this SNP on Glut2 function, we investigated the effects of pharmacological Glut2

and Glut1 inhibition in human T cells purified from blood buffy coats. To this aim, we used the dual inhibitor Phloretin and the Glut1-selective inhibitor STF-31[16].

Proliferation of CD4+ and CD8+ T cells was reduced by both inhibitors (Fig. 8i). However, the dual inhibitor induced a significantly more profound reduction of proliferation by CD8+ than CD4+ T cells, suggesting that Glut2 is a main contributor to CD8+ human T cell proliferation. We subsequently measured ECAR of 4-day activated CD4+ and CD8+ T cells. Inhibition of Glut1 and Glut2 led to a significant decrease of glycolysis in both T cell subsets, although this was more profound when T cells were exposed to Phloretin, indicating a contribution of both transporters to the glycolytic pathway (Fig. 8j-k). Of note, exposure to Phloretin did not reduce the glycolytic flux to the extent observed in murine T cells (Supplementary Fig. 4i-J), raising the possibility that additional Gluts might be operational in human T cells.

Similar to what we observed in mouse T cells, pharmacologic Inhibition of HIF1α led to upregulated expression of Glut2 in CD8+ T cells (Fig. 8l).
Exposure of human T cells to Gal-9 decreased Glut2 expression (Fig 8m) and glycolysis in CD8+ (Fig. 8n) but not CD4+ T cells (Supplementary Fig. 7f).
Finally, antibody-inhibition of Stomatin led to a decrease of Glut 2 expression in both CD4+ and CD8+ T cells (Fig. 8o).
Overall, these data suggest that Glut2 plays a role in human T cell glucose metabolism and like in murine T cells, is regulated by the interplay of HIF1α, Gal-9 and Stomatin.

Figure 8

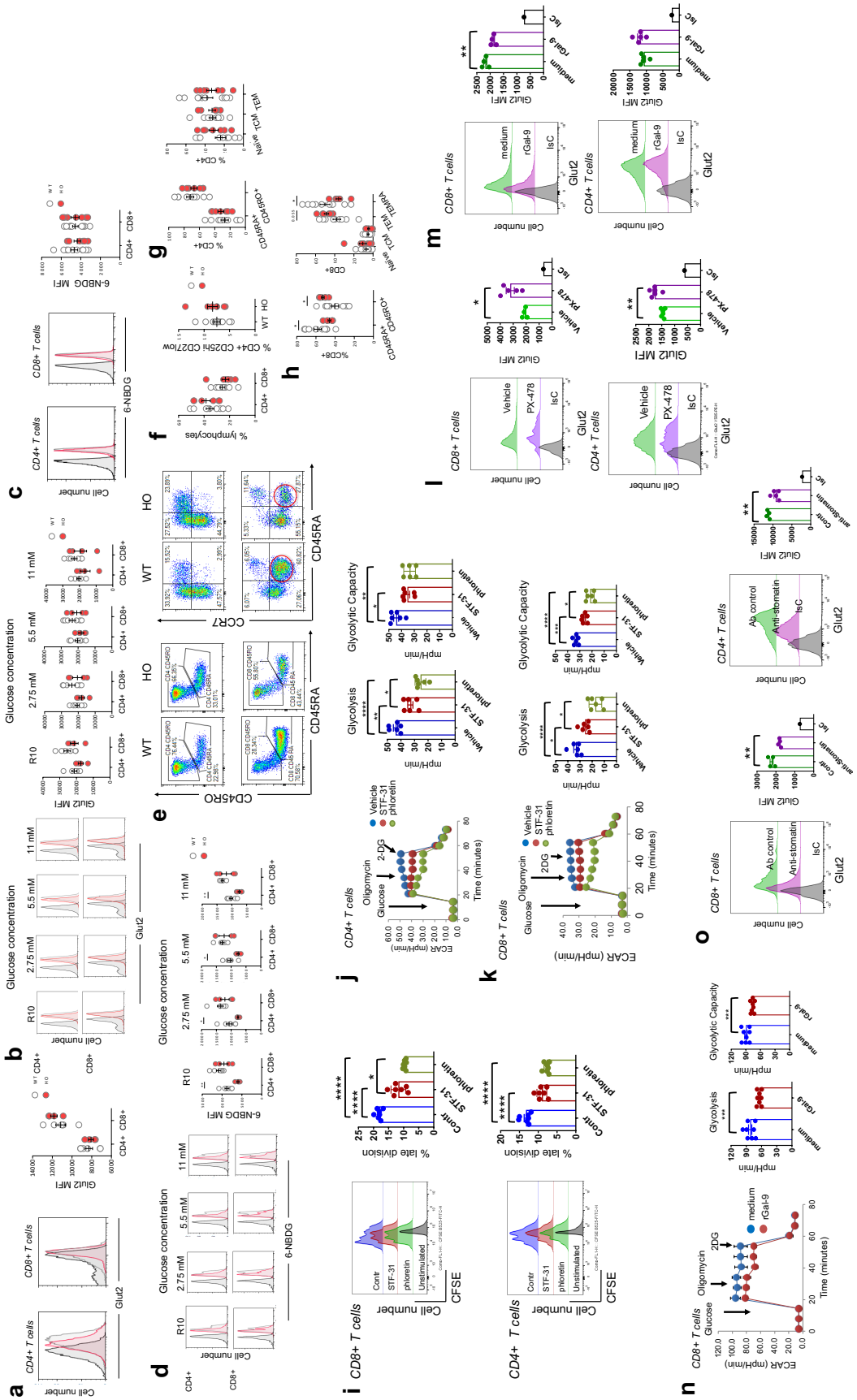

Glut2 is expressed by- and is functional in- human T cells.

(**a-b**) GLUT2 expression and (**c-d**) 6-NBDG uptake were assessed by flow cytometry in CD4+ and CD8+ T cells from wild type (WT) age- and sex-matched homozygous carriers of SLC2A2 snp (HO) ex vivo (**a, c**) or after two days of antibody- activation in complete RPMI (R1) or glucose-free medium reconstituted with 2.75 mM, 5.5 mM or 11 mM of glucose (**b, d**); representative histograms from flow cytometric analysis are shown (grey line represents controls, red line SLC2A2 SNP carriers, black is FMO control staining). Graphs show the mean data measured in the indicated number of individuals ± SEM, n=4-10/group. Unpaired *t*-test.

(**e-h**) Percentage of circulating CD4+ and CD8+ T cells (**e**) and their subsets in wild type and matched age and sex carriers of SLC2A2 snp: regulatory T cells (**f**) (CD4+ CD25hi CD127low); memory CD4 and CD8 T subsets (**g**) (CD45RA+CD45RO- vs CD45RA+CD45RO) and subpopulations (**h**) of naive (CD45RA+CCR7+), central memory (TCM: CD45RA-CCR7+), effector memory (TEM: CD45RA-CCR7-) and terminally differentiated effector memory T cells (TEMRA: CD45RA+CCR7-); representative dot plots from flow cytometry analysis are shown. Unpaired *t*-test.

(**i**) CFSE (5μM) labelled human CD8+ and CD4+ T cells were antibody-activated for 5 days. Glut1 inhibitor (STF-31, 1.25μM) or dual inhibitor (Phloretin, 75μM) or vehicle control was added to cells on day 4 before harvesting on day 5 for flow cytometry. Representative histograms are shown (n = 7), and cumulative data in a representative of 3 experiment of identical design each performed in triplicate is shown (±SD). One-way ANOVA.

(**j**) Extracellular acidification rate (ECAR, mpH/min) in 4-day activated human CD4+ T cells treated with Glut1 inhibitor (STF-31, 1.25μM) or dual inhibitor (phloretin, 75μM) or vehicle control. The bar graph shows the mean glycolysis and glycolytic capacity (±SD, n=5-6). One-way ANOVA.

(**k**) ECAR (pmol/min) in 4-day activated human CD8+ T cells treated with Glut1 inhibitor (STF-31, 1.25μM) or dual inhibitor (phloretin, 75μM) or vehicle control. The bar graph shows the mean glycolysis and glycolytic capacity (±SD, n=5-6). One-way ANOVA.

(**i**) Human naïve T cells were isolated from PBMC, and antibody-activated for 6 days in the presence or absence of the HIF1α selective inhibitor PX-478 (20μM) before analyzing surface expression of Glut2 by flow cytometry. Unpaired *t*-test.

(**m**) Human naïve T cells were antibody-activated for 6 days in the presence or absence of recombinant Gal-9 (30nM) before analyzing surface expression of Glut2 by flow cytometry. Unpaired *t*-test.

(**n**) ECAR (pmol/min) in 4-day activated human CD8+ T cells treated with recombinant Gal-9 (30nM) or vehicle control. The bar graph shows the mean glycolysis and glycolytic capacity (±SD, n=5-6). Unpaired *t*-test.

(**o)** Human naïve CD3 T cells were isolated from PBMC, and antibody-activated for 6 days in the presence anti-stomatin (2.5μg/ml) or isotype control antibody before analyzing surface expression of Glut2 by flow cytometry. Unpaired *t*-test.

*p<0.05, **p<0.01, ***p<0.001, ****p<0.0001.

Discussion

We here report a non-redundant contribution of the glucose transporter Glut2 in the post-priming effector phase of CD8+ T cell-mediated immune responses.

Glut2 promotes CD8+ T cell proliferation, function (IFN-γ and Granzyme-B production) and effector memory differentiation by fuelling the glycolytic pathway during activation. Further, Glut2 appears instrumental to glucose uptake during CD8+ T cell recirculation after priming, likely leading to glycogen synthesis, required for optimal CD8+ T cell function at effector sites, as well as the development of memory and effector function [36]. In line with our findings, efficient glycolysis is required to promote IFN-γ gene expression [17, 18], including in CD8+ T cells [41]. Also, in the absence of glucose, $CD8^+$ T cells have a defect in cytolytic activity marked by reduced granzyme and perforin production [42]. In addition, our data are consistent with reports that attenuation of glycolysis is associated with the development of central memory T cells [43, 44].

The dynamic regulation of Glut 2 expression at different phases and sites suggests a unique role of this glucose transporter in facilitating metabolic adaptation of CD8+ T cells in distinct microenvironments, likely defined by its low affinity for glucose. First, Glut2 is highly expressed by recently primed T cells in the blood, which is rich of glucose and highly oxygenated, and this leads to Glut2-dependent glucose uptake and glycogen accumulation. High glucose uptake and glycogen storage during recirculation are essential to CD8+ T cell survival in inflammatory sites of effector response, as previously reported [36].

In contrast, Glut2 is dramatically downregulated in poorly oxygenated inflammatory sites (inflamed peritoneum and tumour).

Given the ability of low-affinity Glut2 to bidirectionally transport glucose along a concentration gradient, its prompt removal from the cell surface is instrumental to prevent glucose leakage in glucose-depleted inflammatory sites. In contrast, the high affinity glucose transporter Glut1, whose expression does not decrease in inflammatory sites, can sustain glucose uptake and glycolysis in conditions of low glucose availability.

Mechanistically, the different effects of oxygen sensing mediated by the transcription factor HIF1α dominate the differential regulation of Glut2 and Glut1 expression. As both transporters are regulated in a similar manner by glucose concentration and pH, the opposite regulatory outcomes by HIF1α activation on Glut2 and Glut1 expression are instrumental to this complex, yet extremely effective coordinated function of the two transporters which is consistent with their topographic expression.

Intriguingly, while HIF1α directly and positively regulates Glut1 expression at the transcriptional level, inhibition of Glut2 expression is indirect and involves increased Gal-9 production and competition with Stomatin for its localization in rafts at the cell membrane. Following T cell activation in the lymph nodes, Stomatin is upregulated and can compete with Gal-9, thus stabilizing Glut 2 at the cell membrane. In contrast, upregulation of Gal-9 by HIF1α activation outcompetes Stomatin leading to Glut2 downregulation. In this respect, the regulation of Glut2 membrane stabilization follows a similar pattern to that described for pancreatic beta cells [34], albeit with opposite effects, with Gal-9 reducing its expression and Stomatin maintain Glut2 stability at the T cell surface. The molecular basis of the T-cell-specific effects remains to be established, and it is likely to involve interactions of Glut2 with distinct, yet undefined partners in the lipid raft micro domains. In this context, multivalent galectin 3–N-glycan complexes have been shown to reduce TCR clustering by restricting lateral TCR movement within the plane of the membrane, thereby increasing agonist threshold for TCR signalling [45]. Similarly, Glut1 has been shown to interact with Stomatin in adipocytes leading to its translocation in lipid rafts [46]. These interactions were enhanced in glucose deprivation conditions, but did not affect Glut1 ability to uptake glucose, suggesting that Stomatin may also serve as an anchor for Glut1 in lipid rafts.

A summary of these observations in a physiologic context is provided in Supplementary Fig. 8.

The physiological relevance of relative lack of effect of Glut2 deficiency in CD4+ T cells is intriguing. Given that the effect of Galectin-9 on Glut2 expression occurs in antibody-activated CD8+ T cells, it must be assumed that in this subset this effect is operated in an autocrine manner. In contrast, in CD4+ T cells Glut2 expression is downregulated only by addition of exogenous Galectin-9, suggesting that these T cells do not produce sufficient Galectin-9 to elicit autocrine effects. This difference might underlie the fact that CD4+ T cells have adapted their metabolic responses towards a dominant Glut1 function [12].

The relative contribution of these glucose transporters appears to be clearly demarcated by the environmental conditions in which CD4+ and CD8+ T cells develop and exert their effector functions.

In the CD8+ T cell subset, both Glut1 and Glut2 can support the glycolytic pathway. The prominent dependence of CD8+ T cells on Glut2 expression is likely dictated by a combination of requirement for glucose availability and glycolysis to sustain effector responses [5], including glycogen storage [36] for intracellular supply, and the location of activities in severely glucose-depleted microenvironments. It is likely that the role of Glut1, as a transporter that can function in conditions of low glucose availability, plays an auxiliary role when CD8+ T cells localise to glucose-depleted inflammatory sites, and lose Glut2 expression. The relative Glut2 independence of CD4+ T cells might reflect the fact that effector CD4+ T cells carry out a large part of their activities such as cytokine production and help for B cell responses in lymph nodes, which provide a less harsh microenvironment compared to that experienced by effector CD8+ T cells.

The relative contribution of Glut1 and Glut2 in human CD4+ and CD8+ T cell responses is less clear cut. In our pilot study, both glucose transporters equally contribute to T cell glucose uptake, glycolytic activity and T cell division. However, the differential regulation of their expression appears conserved in mice and humans, suggesting that the prominent environment-dependence of the transporters is conserved. Further studies are needed to fully resolve these discrepancies.

A limitation of our study lays in the fact that the Glut2-deficient chimeras are not T cell-specific. Although we tried to mitigate this issue at the best of our ability (i.e. adoptive transfer of purified T cells, studies of antigen presentation in vivo and of cell-intrinsic defects in vitro), studies with T cell-specific knockouts of Glut2, Glut1 and both transporters are needed to validate our observations.

Finally, the present study fully supports the notion that in vitro studies of metabolism need to reproduce the environmental cues that T cells encounter in vivo, during recirculation in different tissues compartments [47]. For example, Glut2 expression cannot be detected in murine T cells kept in conventional tissue culture media, which contains too high a glucose concentration (10-25mM) for its expression. As we have shown, glucose availability and oxygen concentration and pH are other parameters that should be considered when studying metabolic adaptation of T cells, which in physiology constitutively and continuously visit different microenvironments, *in vitro*.

Methods

Study design

This study describes a non-redundant role of Glut2 in the regulation of CD8+ T cell responses. The study aimed at defining the contribution of Glut2 to T cell metabolism and function using in vitro and in vivo study in mice and in vitro assays in humans. Several phenotypic and functional assays were employed to assess the ability of Glut2 to uptake glucose and engaging the glycolytic pathway, and the regulation of its expression by different microenvironment. Mechanistic studies also involved the use of genetically modified mice.

Animals

C57BL/6 and BALB/c mice were purchased from Charles River (UK). Ripglut1;glut2-/- mice (Referred to as Glut2-) were kindly provided by Bernard Thorens (University of Lausanne, Switzerland) [15]. B6.Kd (BL/6 transgenic for Kd) were a gift from Robert Lechler (King's College London). B6.129-Hif1atm3Rsjo/J (HIFaloxp) and B6.Cg-Tg(Cd4-cre)1Cwi/BfluJ mice were purchased from Jackson Laboratory. Galectin-9 knockout mice (B6(FVB)-Lgals9tm1.1Cfg/Mmucd) on a C57BL/6J background were obtained from the Mutant Mouse Resource and Research Centers, USA (originally deposited by J Paulson, The Scripps Research Institute, USA). Female Marilyn mice, bearing a transgenic TCR specific for the male minor transplantation antigen HY peptide epitope Dby (NAGFNSNRANSSRSS) and restricted by H2-Ab molecules, have been previously described [21]. Mata Hari mice, bearing a transgenic TCR specific for the male minor transplantation antigen HY peptide epitope Uty (WMHHNMDLI) and restricted by H2-Db molecules, have been previously described [20]. Mice were fed a regular chow diet and used at the age of 8-12 weeks. Littermates of the same sex were randomly assigned to experimental groups. In experiments assessing T cell response to HY antigen only female mice were used. All *in vivo* experiments were conducted with strict adherence to the Home Office guidelines (PPL P71E91C8E) and approved by the local Ethics Committee.

Human study.

Human blood was obtained from healthy donors from the Progressione della Lesione Intimale Carotidea (PLIC) Study (a sub-study of the CHECK study), a large survey of the general population of the northern area of Milan (n= 2.606) [48] followed at the Center for the Study of Atherosclerosis, Bassini Hospital (Cinisello Balsamo, Milan, Italy). The Study was approved by the Scientific Committee of the Università degli Studi di Milano ("Cholesterol and Health: Education, Control and Knwoledge – Studio CHECK ((SEFAP/Pr.0003) – reference number Fa-04-Feb-01) in February 4th 2001. An informed consent was obtained by subjects in accordance with the Declaration of Helsinki.

Genomic DNA was extracted using Flexigene DNA kit (Qiagen, Milan,Italy). Samples from the PLIC study were genotyped for the rs5400 missense mutation (G>A allelic change; https://www.ncbi.nlm.nih.gov/snp/rs5400) on the *SLC2A2* locus, by TaqMan-based allelic discrimination. 58 homozygous AA were found versus 209 GA heterozygous and 711 wild-type GG (Hardy-Weinberg, chi-squared= 51.189). The experimental analysis was conducted on a subgroup of 17 subjects, ten GG (*wild type*) and seven AA (*homozygous*) matched by age, sex and clinical and pharmacological history. Body Mass Index (BMI, Kg/m2) was calculated and the determination of plasma lipid profile, glucose levels, liver enzymes and whole blood leukocytes counts were available after an over-night fast (at least 10 hours) with a blood drawn from antecubital vein. Supplemental Table 1 reports these parameters.

Human blood was obtained from healthy donors according to ethical approval from the Università degli Studi di Milano (Cholesterol and Health: Education, Control and Knowledge – Studio CHECK [SEFAP/Pr.0003] – reference number Fa-04-Feb-01).

Generation of chimeric mice

WT C57BL/6 mice were sub-lethally irradiated with 2 doses of 4Gy x-ray delivered 4 hours apart. 18h after the 2nd dose of irradiation they were reconstituted with 3×10^6 bone marrow cells that had been harvested from the femurs and tibias of age-matched wild-type or

Ripglut1;glut2-/- (Referred to as Glut2-) mice respectively. After 8 weeks, mice were tested for chimerism by RT-PCR for protein expression by T cells.

Reagents

Unless otherwise indicated, all the experiments described here have been performed in media supplemented with 5mM glucose.

CFSE was purchased from Invitrogen and used at 5μM. PX-478 was purchased from Cayman chemical. Glucose glutamine free T cell medium was purchased from MP Biomedicals. 6-NBDG and Pierce™ 16% Formaldehyde (w/v) were purchased from ThermoFisher. Dulbecco's Modified Eagle media (DMEM) was purchased from Merck. RPMI, glutamine, 2-Mercaptoethanol (2-ME), sodium pyruvate and HEPES were purchased from Gibco. Glucose, 2-Deoxy-D-glucose, oligomycin A, FCCP, rotenone, antimycin, red blood cell lysis buffer, DAPI (4',6-Diamidino-2-Phenylindole, Dihydrochloride) and dithiothreitol were purchased from Sigma-Aldrich; FBS was purchased from Seralab. Ficoll-PlaqueTM PREMIUM was purchased from GE-Healthcare. GolgiPlug was purchased from BD biosciences. High-Capacity RNA-to-cDNA™ Kit, ProLong Gold Antifade and LIVE/DEAD™ Fixable Aqua Dead Cell Stain Kit were purchased from Life Technologies. Intracellular Fixation & Permeabilization Buffer Set was purchased from eBioscience. TaqMan human L 750 uL 80X – assay ID: C___2862880_1_ and TaqMan™ Genotyping Master Mix were purchased from Applied Biosystem. FlexiGene DNA kit (250 reactions) and RNeasy Mini Kit (50) were purchased from Qiagen. iQ™ SYBR® Green Supermix was purchased from Biorad. Murine IFNγ (clone H22), MojoSort™ Mouse CD8 T Cell Isolation Kit and MojoSort™ Mouse CD4 T Cell Isolation Kit were purchased from Biolegend. Mouse naive CD4 T cell isolation kit, Mouse CD4 T cell isolation kit and Mouse CD8 T cell isolation kit were purchased from STEMCELL. EasySep™ Human Naïve Pan T Cell Isolation Kit were purchased from STEMCELL. MojoSort™ Human CD8 T Cell Isolation Kit and MojoSort™ Human CD4 T Cell Isolation Kit were purchased from Biolegend. XF assay medium, Seahorse XF Cell Mito Stress Test Kit and Seahorse XF Glycolysis Stress Test Kit were purchased from Agilent Technologies. CD8 depletion antibody (clone 2.43) was

purchased from BioXCell. Recombinant murine IP-10 (250-16) and recombinant murine IFNγ (315-05) were purchased from PeproTech. Recombinant murine Galectin-9 (3535-GA-050) was purchased from R&D SYSTEMS.

The Glut1 inhibitor STF-31 (SML1108) and the dual Glut1 and Glut2 inhibitor Phloretin (P7912) were purchased from Sigma Aldrich. Optimal doses were determined from available literature as well as titration followed by measurement of ECAR in activated T cells.

Antibodies

For the phenotypic characterization of murine studies, cells were stained with: CD25 PE (clone PC61.5); CD26 PerCP/Cy5.5 (clone H194-112); CD28 PE (clone 37.51); CD31 PE/Cy7 (clone 390); CD38 PE/Cy7 (clone 90); CD44 pacific blue or BV605 (clone IM7); CD45.1 FITC (clone A20); CD45.2 AF700 (clone 104); CD49d PE (clone 9C10); CD62L FITC (clone MEL-14); CD69 FITC (clone H1.2F3); Glut1 AF647 (clone EPR3915) or AF 405 (polyclonal); Glut2 PE (clone 205115); Gal-9 APC (clone 108A2) or PE/Cy7 (clone RG9-35); Stomatin AF488 (polyclonal); MHCI (H-2kb/H-2Db) AF647 (clone 28-8-6); TCRβ BV605 (clone H57-597); CCR4 APC (clone 2G12); CCR5 PE (clone HM-CCR5); CCR6 PE (clone 29-2L17); CCR7 APC (clone 4B12); CXCR3 PerCP/Cy5.5 (clone CXCR3-173); CXCR4 FITC (clone 2B11/CXCR4); LFA-1 PE/Cy7 (clone M17/4); B220 BV605 (clone RA3-6B2); CD107α PE/Dazzle 594 (clone 1D4B);

Phenotypic characterization of human cells was performed with: CD3 AF700 (clone UCHT1); CD4 BV605 (clone SK3, also known as Leu3a); CD8 ef450 (clone SK1); CD8 FITC (clone RPA-T8); CCR7 FITC (clone REA546); CD45RA-BV785 (clone HI100); CD45RA-PerCPVio700 (clone REA1047); CD45RO- APCVio770 (clone REA611); Glut2-PE (clone 199017)

Intracellular staining for murine studies was performed with the following antibodies: FoxP3 APC (clone FJK-16s); Hif1α FITC or PE (clone 241812); Granzyme B FITC (clone GB11);

IFNγ PerCP/Cy5.5 (clone XMG1.2); IL-17 ef450 (clone eBio17B7). IFNγ AF647 (clone B27) was used for intracellular cytokine staining in human cells.

Cell surface staining

For surface staining, cells were resuspended (10^7/ml) and stained with flurochrome-conjugated antibodies in 100µl of Flow cytometry buffer (PBS containing 1% FBS and 0.1% sodium azide) at 4°C for 30 minutes. CCR7 antibody staining was performed at 37°C for 30 minutes. Optimal antibody concentrations for staining were calculated based on manufacturer instructions. Following staining, cells were washed and resuspended with flow cytometry buffer and analyzed immediately. Alternatively, for delayed analysis, cells were fixed in fixation buffer (flow cytometry buffer containing 1% formaldehyde) for 30 minutes at 4°C, washed and stored in flow cytometry buffer at 4°C.

Samples were acquired on a LSRII Fortessa flow cytometer (BD Biosciences, San Jose, California, USA) equipped with 405, 488, 560 and 641nm lasers, BD cytometer setup and tracking beads were routinely used to calibrate the cytometer. Single stain and fluorescence minus one controls were acquired for compensation and precise gating, respectively. Compensation was automatically calculated, and samples analyzed on dedicated software (FlowJo version 10, FlowJo LLC, Oregon, USA). Analysis was performed on the same day of acquisition.

Intracellular cytokine staining

For stimulating cytokine production, T cells (2×10^6/ml) were re-stimulated with 50 ng/ml phorbol 12-myristate acetate (PMA) and 500 ng/ml ionomycin in the presence of 500µg/ml brefeldin A for at least 4 hours. Cells were first stained with antibodies for surface molecules. After washing, cells were fixed and permeabilized with intracellular fixation & permeabilization buffer for at least 30 minutes. Cells were then washed and resuspended in 1X perm solution containing antibodies for intracellular cytokines or isotype-matched control antibodies. After a final wash, the cells were resuspended in staining buffer for flow cytometry analysis.

Antibody-mediated T cell activation

T cells were stimulated with plate-bound anti-CD3 (1 µg/ml, eBiosciences, 16-0032-85) and anti-CD28 (5 µg/ml, eBiosciences, 16-0281-86) in cell medium supplemented with 20 U/ml recombinant IL-2 (Roche, 10799068001), sometimes with different concentrations of glucose or different Ph levels for various periods of time according to experimental purposes (see figure legends). To evaluate the effect of oxygen, T cells were antibody-activated antibodies for two days, then transferred into incubators either containing 20% oxygen or 5% oxygen (Baker Ruskinn InvivO2 400 hypoxic workstation) overnight before analysis.

In experiments investigating the effect of pH on Glut2 expression, various volumes of 1 M HCl were added to the medium until the desired pH was obtained. Prior to use in experiments, the medium pH was checked after 24 h of incubation at 37 °C under 5% CO_2.

In polarization studies, CD8+ T cells were isolated from WT and Glut2-deficient mice, activated by plate bound CD3/CD28 Abs, and differentiated toward Tc-0 and Tc-1 phenotypes by culture with 10ng/mL IL-2 (Tc-0) or 10ng/mL IL-2; 5ng/mL IL-12 (BioLegend, 577002) and 2µg/mL anti–IL-4 (BioLegend, 504102)(Tc-1).

T cell intravital labelling

For labelling T cells with fluorescent probes, T cells were washed with PBS, counted and resuspended in PBS at a final concentration of 10^7/ml. Labeling of T cells with succinimidyl ester dyes CFSE was performed by incubating T cells in PBS containing final concentration of 5µm CFSE for 10-15 minutes at room temperature. The reaction was terminated by adding equal volume FBS and the cells were then washed with PBS.

Measurement of ECAR and OCR

Real time bioenergetics analysis of extracellular acidification rates (ECAR) and oxygen consumption rates (OCR) of T cells was performed using the XF analyzer (Seahorse

biosciences). Murine CD8+ and CD4+ T cells were isolated and antibody-activated for 2 days. Human CD8+ and CD4+ T cells were isolated from PBMC and antibody-activated for 5 days. Glut1 inhibitor (STF-31, 1.25μM) or Glut2 inhibitor (phloretin, 75μM) or vehicle control was added to cells during 1 hour incubation time before Seahorse assay. Recombinant Gal-9 (30nM) or vehicle control was added to cells 1 day before and during the Seahorse assay. T cells were seeded (3-5 x 10^5 /well) into the seahorse XF96 cell plates for analysis. Perturbation profiling of the use of metabolic pathways by T cells was achieved by the addition of oligomycin (1 μM), FCCP (1 μM), antimycin A (1 μM), rotenone (1 μM), D-glucose (10mM), 2-Deoxy-D-glucose (2DG, 50mM). Metabolic parameters were calculated.

Metabolic labeling and metabolome analysis

Naive CD8+ T cells were isolated from Glut2+ and Glut2- mice and cultured on anti-CD3/CD28 coated cell culture plates in glucose-free RPMI supplemented with 2.5mM glucose for 48 hours, and the cell media was then changed to media containing 5mM 13C6-glucose (Cambridge Isotope Laboratories, CLM-1396-5) and cultured for an additional 18 hours before isolation of metabolites. Briefly, cells were washed with PBS 3 times and resuspended in ice cold extraction buffer (50% methanol, 30% acetonitrile, 20% ultrapure water) at a ratio of 20 × 10^6 cells/mL. Cells were incubated on methanol and dry ice for 15 minutes and then placed on a shaker for 15 minutes at 4°C, followed by incubation at –20°C for 1 hour. Cell lysate was centrifuged, and the supernatant collected and transferred to autosampler glass vials which were stored at –80°C until further analysis.

LC-MS/MS analysis was performed using a Q Exactive Quadrupole-Orbitrap mass spectrometer coupled to a Vanquish UHPLC system (Thermo Fisher Scientific) as described previously. The liquid chromatography system was fitted with a Sequant ZIC-pHILIC column (150 mm × 2.1 mm) and guard column (20 mm × 2.1 mm) from Merck Millipore and the temperature maintained at 35°C. The sample (2 μL) was separated at a flow rate of 0.1 mL/min. The mobile phase was composed of 10 mM ammonium carbonate and 0.15%

ammonium hydroxide in water (solvent A) and acetonitrile (solvent B). A linear gradient was applied by increasing the concentration of A from 20% to 80% within 22 minutes and then maintained for 7 minutes. The mass spectrometer was operated in full MS and polarity switching mode, in the range of 70–1000 m/z and resolution 70,000. Major ESI source settings were: spray voltage 3.5 kV, capillary temperature 275°C, sheath gas 35, auxiliary gas 5, AGC target 3e6, and maximum injection time 200 ms. For the targeted analysis, the acquired spectra were analyzed using XCalibur Qual Browser and XCalibur Quan Browser software (Thermo Fisher Scientific). Compound discoverer 3.1 (Thermo Fisher Scientific) was used for untargeted and potentially novel feature detection and annotation with library scoring. Features with the fold change greater than 2 and $P < 0.05$ were selected as discriminating markers. Samples were analyzed by quadruplicate.

Quantitative Real-Time Polymerase-Chain Reaction (qRT-PCR)

RNA was purified using Qiagen RNAeasy Kit according to the manufacturer's instructions. Reverse transcription was performed according to the manufacturer's instruction (Applied Biosystems). Gene expression analysis was done using SYBR Green Supermix (Biorad) in CFX connect light cycler (Biorad), according to the manufacturer's instructions. The qPCR data were analyzed using the delta delta CT method by taking the CT values of the genes of interest from the house keeping gene. Data were exported to Prism before graphic presentation and statistical analysis.

The following primers were used: a-tubulin: TCTCGCATCCACTTCCCTC (forward) and ATGCCCTCACCCACGTAC (reverse); 18s rRNA: GCAATTATTCCCCATGAACG (forward) and GGCCTCACTAAACCATCCAA (reverse); Aconitase: ATCGAGCGGGGAAAGACATAC (forward) and TGATGGTACAGCCACCTTAGG (reverse); Oxoglutarate: TATGGCCTACACGAGTCTGAC (forward) and CCAGCCGACGGATGATCTC (reverse); Fumarase: GAATGGCAAGCCAAAATTCCTT (forward) and CGTTCTGTAGCACCTCCAATCTT (reverse); Malate dehydrogenase:

TTCTGGACGGTGTCCTGATG (forward) and TTTCACATTGGCTTTCAGTAGGT (reverse); Glut1: CACTGTGGTGTCGCTGTTTG (forward) and ATGGAATAGGACCAGGGCCT (reverse); Glut2: CCTACTTGGCCTATCTGCTGT (forward) and GCCCTGACTTCCTCTTCCAA (reverse); Glut3: TCGGATGTCACAGGAGAAGC (forward) and CTGAGACAGCTGGAGGACAA (reverse); Glut6: AACCGAGGGACTCGACTATGA (forward) and CAAGGCATACCCAAAGCTGAA (reverse); Glut8: CCCTTCGTGACTGGCTTTG (forward) and TGGGTAGGCGATTTCCGAGAT (reverse); Gal-9: ATATCAACCTTCGCTGTGGAGG (forward) and CCCCAGGAGTTGTTGATCTG (reverse); Stomatin: CAGATTCAGCAACCCGTCTTT (forward) and GTCCAGCGTACTCTGCATGTG (reverse); Hexokinase I: TCACATTGTCTCCTGCATCTC (forward) and CTTTGAATCCCTTTGTCCACG (reverse); Hexokinase II: TCAAAGAGAACAAGGGCGAG (forward) and AGGAAGCGGACATCACAATC (reverse); PFKFB3: CTGACTCGCTACCTCAACTG (forward) and ACTGTTTTCGGACTCTCATGG (reverse); Pkm2: CCATTCTCTACCGTCCTGTTG (forward) and CCATGTAAGCGTTGTCCAG (reverse); PDHA1: ACATGGCTTCACCTTCACTC ((forward) and CCGTTGCCTCCATAGAAGTTC (reverse); CPT-1α: CCAAGTATCTGGCAGTCGA (forward) and CGCCACAGGACACATAGT (reverse); Hif1α: TCTGAACGTCGAAAAGAAAAGTC (forward) and ACGTAAATAACTGATGGTGAGCC (reverse); Granzyme B: CCACTCTCGACCCTACATGG (forward) and GGCCCCCAAAGTGACATTTATT; IFN-γ: TCAAGTGGCATAGATGTGGAAGAA (forward) and TGGCTCTGCAGGATTTTCATG (reverse); T-bet: CCTCTTCTATCCAACCAGTATC (forward) and CTCCGCTTCATAACTGTGT (reverse).

In vitro 6-NBDG uptake assay

T cells were washed in PBS and resuspended in glucose free T cell medium for 1 hour before a final concentration of 60 μM 6-NBDG in glucose free T cell medium was added to the cells. Cells were further incubated for an additional 30 minutes. Finally, the cells were washed twice

with warm PBS and resuspended in flow cytometry buffer and placed on ice. Immediate analysis was performed using flow cytometry to observe 6-NBDG uptake by the T cells.

***In vivo* 6-NBDG uptake assay**

Mice were starved for 2 hours before injection of 6-NBDG at 5mg/Kg. Cells were further incubated for an additional 30 minutes. T cells were then washed twice with warm PBS and resuspended in flow cytometry buffer and placed on ice. Flow cytometric analysis was performed immediately.

***In vivo* proliferation**

T cells from Marilyn mice (10^7/mouse) and Mata Hari mice (10^7/mouse) were labeled with CFSE (5 μM) and injected intravenously into Glut2+ and Glut2- female recipients. Twenty-four hours later, recipient mice received a IP injection of male splenocytes ($5x10^6$). Five days after immunization, T cells were separately harvested from mesenteric LN (draining LN, dLN), inguinal and axillary (non-draining LNs, ndLN) and the spleen. CFSE dilution in Marilyn T cells (CD4+Vb6+CD45.2+) and Matahari T cells (CD8+Vb8.3+CD45.2+) was assessed by flow cytometry.

***In vivo* Glut2 and Glut1 Expression**

Purified CD45.2+ Mata Hari CD8+ T cells (MH) were adoptively transferred into CD45.1+ recipients, which were then immunized with male HY antigen on day 1 and day 4, followed by IP injection of 1.2 μg of IP-10 on day 4. PBMC were harvested from tail blood at different time points, and T cells were separately harvested from peritoneum, spleen, mesenteric LN (draining LN, aLN), and axillary LN (non-draining LN, ndLN) on day 5. Expression of Glut2 and Glut1 by donor MH T cells (identified as CD8+Vb8.3+CD45.2+.) and recipient CD8+ T cells (identified as CD8+CD45.1+CD45.2-) were assessed by flow cytometry.

Immunization with ovalbumin.

Mice were primed and boosted with IP injection of 750μg ovalbumin protein plus 50μg Poly(I:C) adjuvant or adjuvant alone as control. After 7 days, T cells were separately harvested from mesenteric LN (draining LN, dLN), inguinal and axillary (non-draining LNs, ndLN) and the spleen. Expression of IFN-γ, Granzyme B, and IL-17 were assessed by flow cytometry.

Glycogen quantification using the Glycogen Assay Kit

Glycogen levels were measured using the Glycogen Assay Kit (MERCK) following the manufacturer's instructions. Briefly, 1×10^6 day 3-activated T cells were homogenized with 200 µl H2O on ice and then boiled for 10 minutes. Homogenates were spun at 20,000 g for 10 minutes and supernatants were assayed for glycogen content. Results were normalized by protein content.

Glycogen quantification by transmission electron microscope

Naïve Glut2+ and Glut2- CD8+ T cells were purified, antibody-activated for 4 days and harvested for imaging of Glycogen by transmission electron microscope. Briefly, cell samples were embedded in 2% (w/v) low-gelling temperature agarose, cut in 1–2 mm cubic blocks, and fixed with 2% (w/v) potassium permanganate dissolved at 4°C overnight. Samples were washed with distilled water and dehydrated through a graded ethanol series. Samples were then washed twice with propylene oxide prior infiltration with Araldite for 1 hour and with fresh Araldite overnight. Polymerization was achieved by incubation at 60–65°C for 48 hours. Alternatively, cells were fixed at room temperature for 2 hours in 100 mM phosphate buffer pH 7.0 containing 0.5% (w/v) tannic acid, 1% (w/v) formaldehyde, and 3% (w/v) glutaraldehyde, washed with phosphate buffer, and incubated in 2% (w/v) OsO4 in phosphate buffer overnight. Dehydration was performed using a graded acetone series. Thin sections were cut with a glass knife at a Reichert Ultracut E microtome and collected onto uncoated 300 mesh copper grids. High contrast was obtained by post-staining with saturated aqueous

uranyl acetate and lead citrate for 4 minutes each. The grids were examined in a JOEL JEM-1230 transmission electron microscope. Areas for glycogen deposits and the whole cell were quantified and analysed via QuPath V0.43 and Graphpad 9 softwares.

***In vivo* glucose leakage in inflamed non-lymphoid tissue.**

Purified CD45.2+ HIF-1α-competent or -deficient naïve CD8+ T cells (107) were antibody-activated for 3 days, labelled with 6-NBDG and injected IP in CD45.1+ syngeneic mice which had received a IFN-γ (300ng) injection IP 48 hours previously. 6-NBDG in CD8+ T cells was measured by flow cytometry before and 30 minutes after injection. 6NBDG concentration in peritoneal fluids was measured by a fluorescence plate reader 30 minutes after injection.

Skin grafting

Donor tail skin was removed and cut into 1cm^2 sections. Recipient mice were anesthetized using isoflurane (Halocarbon Products Corp.). A piece of skin was removed from the right flank to create a graft bed, and a 1cm^2 piece of tail skin was placed in the graft bed. The graft was covered with muslin, and a plaster cast was wrapped around the midriff and graft. Plasters were removed 7–9 days after grafting. Skin graft rejection was assessed as previously described [49].

E0771 tumor cell implantation

Murine E0771 mammary adenocarcinoma cells were grown in RPMI 1640 Medium (Gibco) supplemented with 10 % FBS (Gibco) and 1 % penicillin–streptomycin (Gibco). Cells were kept at 37 °C in a humidified incubator in the presence of 5% CO2. For orthotopic implantation as a syngeneic mouse model of breast cancer, E0771 cells (4 x 10^5) were re-suspended in a 1:1 ratio of PBS and growth-factor reduced Matrigel (Corning) (50 µl total volume and injected into the right fourth inguinal mammary gland of female glut2 WT or KO chimera C57BL/6 mice.

Tumour growth was monitored every 2 – 3 days after tumours became palpable by measuring tumour length and width using callipers. Tumor volumes (mm3) were calculated using the formula: (width)2 × length/2, where width is the smaller of the two measurements. Animals were sacrificed at various days in compliance with project licence with limit on tumor size. At 28 days, tumors were harvested and volume measured. Pieces of tumor tissue were embedded in either OCT or formalin for histological examination while other pieces of were digested enzymatically using collagenase to generate single-cell suspensions for flow cytometry staining.

Nuclei isolation and staining.

Splenic T cells were isolated from C57BL/6 mice and seeded in 24-well plate in RPMI 1640 containing 2% FBS. Cells were incubated at 37ºC degree in incubators containing either 20% oxygen or 5% oxygen for 24 hours before isolation of nuclei [50].

T cells were then pelleted by centrifugation, then resuspended in the cell lysis buffer (10 mM HEPES; pH 7.5, 10 mM KCl, 0.5 mM EDTA, 1% Triton-X 100, to which 1 mM dithiothreitol and 0.5 Phenylmethylsulfonyl fluoride were added just before use), placed on ice for 15-20 min with intermittent mixing by vortex to disrupt cell membranes. Nuclei were washed twice with the cell lysis buffer and subsequently resuspended in Fix/Perm buffer for at least 30mins before antibody staining.

Imaging

Naïve T cells were allowed to adhere onto coverslip for 30 minutes at room temperature. Activated T cells for staining were obtained by seeding naïve T cells ($1.0x10^6$ cells/well) onto coverslips pre-coated with CD3 (1ug/ml) and CD28 (5ug/ml) in 24 well plates and cultured for 3 or 5 days. Cells were spun down with 200g for 1 minute, followed by fixing with 2% PFA for 20 minutes at room temperature. Cells were then washed with PBS and blocked with blocking buffer (1% BSA and 5% goat serum) for 2 hours at room temperature. After blocking the cells were labelled with appropriate antibodies in the same blocking buffer for 48 hours at +4°C in

the dark. After multiple PBS washes coverslips were mounted onto slides with Fluoroshield and then examined using Zeiss Z1 deconvolution microscope (Carl Zeiss) equipped with an AxioCam MRm cooled monochrome digital camera and an ApoTome.2 imaging unit. Some images were examined using a Leica SP5 confocal microscope. Confocal images and Z stacks were acquired and analyzed by Leica LAS software. Images were acquired using 63 x 1.4 NA (oil) objective.

The corrected total cell fluorescence was measured by ImageJ software and it is calculated based on the following formula:

CTCF = Integrated Density – (Area of selected cell X Mean fluorescence of background readings).

Colocalization analysis and quantification was performed by using Coloc2 and Colocalization Threshold plugins. In short, two channels were selected, and region of interest (ROI) was then highlighted by selection/drawing tool in both channels to measure colocalization in the chosen ROI. The value of volume % was used to calculate the colocalization of the two channels.

Blood surface and intracellular staining (human study)

For surface staining, 100µL of whole blood were stained with fluorochrome-conjugated antibodies in 50µL of MACS buffer made of PBS containing, 2% FBS and 2µM EDTA at RT (room temperature) for 30 minutes in the dark. Optimal antibody concentrations for staining were calculated based on manufacturer instructions. Following staining, red blood cells were lysed with 2 mL of 1-step fix/lyse solution for 20 minutes at RT, washed and resuspended with MACS buffer and analysed immediately.

Alternatively, for intracellular staining, cells were fixed and permeabilized following manufacturer instruction (Cat#555028).

PBMC isolation (human study)

For each subject, 30 mL of blood (supplemented with EDTA) were split in two falcons of 15 mL and spin for 12 minutes at 1000xg. Plasma was discarded and the interface between

plasma and red blood cells, enriched in leukocytes and platelets (buffy coat), was carefully collected, diluted with cold PBS and stratified on 3 mL of Ficoll-Plaque^{TM} PREMIUM. After centrifugation of 35 minutes at 250xg, PBMC layer was carefully collected and was 3 times with 10 mL of cold PBS at 180xg for 12 minutes to get rid of platelets. PBMC were counted and used for subsequent analysis.

In vitro T cell activation, proliferation and IFNγ production (human study).

Freshly isolated PBMC were plated 0,25 x 10^6/200 µL of complete RPMI (Euroclone, ECM9006) or DMEM (Merck, D5030) at 2.75mM, 5.5 mM or 11 mM glucose in 96-well plate U-bottom previously coated with αCD3 (5µg/mL. Invitrogen, 14-0039-82) and αCD28 (2µg/mL, Invitrogen, 14-0289-82) in the presence of rhIL-2 (25U/mL, Roche, 10799068001) for 2 or 6 days according to experimental purposes (see figure legends).

For tracing T cell proliferation, PBMC were stained with 5µm of CFSE for 10 minutes at RT and washed 3 times in 1x PBS/2% FBS/2mM EDTA. Cells were plated for 6 days and thereafter stained with human anti-CD4-BV605 (BD Biosciences, 565998) and anti-CD8-ef450 (Invitrogen, 48-0087-42).

For IFNγ production, PBMC were stimulated as described above for 2 or 6 days, followed by a restimulation with soluble αCD3 (2.5µg/mL) and αCD28 (1µg/mL) in the presence of brefeldin (MERCK, 555028) for 4 hours. Cells were then stained with superficial human anti-CD4-BV605 and anti-CD8-ef450 and intracellular anti-IFNγ-Af647 according to manufacturer instruction (BD Biosciences, 557729).

In vitro 6NBDG uptake assay (human study)

Freshly isolated (ex vivo) or in vitro activated (as detailed above) PBMC were washed in PBS and resuspended in glucose free DMEM. A final concentration of 400µM 6-NBDG in glucose free medium was then added to the cells and the cells were further incubated for an additional 15 minutes at 37°C. Finally, cells were washed twice with warm PBS, stained with anti-CD4

and CD8 fluorescent antibodies and immediately analysed by flow cytometry. 6-NBDG uptake was detected as increased fluorescence in the 530/30 channel.

Statistical analysis

Results are expressed as mean SD (standard deviation) or mean SEM (standard error of the mean). Unpaired student's t-test, one-way ANOVA and Long-rank (Mantel-Cox) test were used as specified in the figure legends. N indicates number of experiments, n indicates number of biological replicates in each experiment, or number of mice/group. All reported p-values are two-sided. A p value of < 0.05 was regarded as significant. Statistical analysis was carried out using Prism.

Acknowledgements

Funding: British Heart Foundation: RG/20/8/34995, CH/15/2/32064, AA/18/5/34222.

Author Contributions

Conceptualization: FMB, GDN, DMS
Methodology: HF, JV, SF, FB, ADA, GW, DL, RC, PG, MS, DT, BT, AI
Investigation: HF, JV, SF, FB, ADA, GW, TP, DL, RC, RJH, PG, MS, SS, VM
Visualization: HF, JV, SF, FB, ADA, GW, DL, RC, PG, MS
Funding acquisition: FMB
Project administration: FMB
Supervision: FMB, DN, ADA, MPL, ES, MB, DMS, DC, GDN, MB, SG, JR, KB
Writing – original draft: HF, JV, SF, FB, MF, GDN, FMB

Competing interests

Authors declare that they have no competing interests.

Data and materials availability:

All data will be made available upon reasonable request by FMB, HF, JV, SF, GDN, FB

References

1. Geltink, R.I.K., Kyle, R.L. & Pearce, E.L. Unraveling the Complex Interplay Between T Cell Metabolism and Function. *Annu Rev Immunol* **36**, 461-488 (2018).
2. Asnagli, H. & Murphy, K.M. Stability and commitment in T helper cell development. *Curr Opin Immunol* **13**, 242-247 (2001).
3. Halle, S., Halle, O. & Forster, R. Mechanisms and Dynamics of T Cell-Mediated Cytotoxicity In Vivo. *Trends Immunol* **38**, 432-443 (2017).
4. MacIver, N.J., Michalek, R.D. & Rathmell, J.C. Metabolic regulation of T lymphocytes. *Annu Rev Immunol* **31**, 259-283 (2013).
5. Cao, Y., Rathmell, J.C. & Macintyre, A.N. Metabolic reprogramming towards aerobic glycolysis correlates with greater proliferative ability and resistance to metabolic inhibition in CD8 versus CD4 T cells. *PLoS One* **9**, e104104 (2014).
6. Thorens, B. & Mueckler, M. Glucose transporters in the 21st Century. *Am J Physiol Endocrinol Metab* **298**, E141-145 (2010).
7. Mueckler, M. & Thorens, B. The SLC2 (GLUT) family of membrane transporters. *Mol Aspects Med* **34**, 121-138 (2013).
8. Swainson, L. *et al.* Glucose transporter 1 expression identifies a population of cycling CD4+ CD8+ human thymocytes with high CXCR4-induced chemotaxis. *Proc Natl Acad Sci U S A* **102**, 12867-12872 (2005).
9. Jacobs, S.R. *et al.* Glucose uptake is limiting in T cell activation and requires CD28-mediated Akt-dependent and independent pathways. *J Immunol* **180**, 4476-4486 (2008).
10. Frauwirth, K.A. *et al.* The CD28 signaling pathway regulates glucose metabolism. *Immunity* **16**, 769-777 (2002).
11. Nath, M.D., Ruscetti, F.W., Petrow-Sadowski, C. & Jones, K.S. Regulation of the cell-surface expression of an HTLV-I binding protein in human T cells during immune activation. *Blood* **101**, 3085-3092 (2003).
12. Palmer, C.S. *et al.* Regulators of Glucose Metabolism in CD4(+) and CD8(+) T Cells. *Int Rev Immunol* **35**, 477-488 (2016).
13. Uldry, M., Ibberson, M., Hosokawa, M. & Thorens, B. GLUT2 is a high affinity glucosamine transporter. *FEBS Lett* **524**, 199-203 (2002).
14. Prentki, M., Matschinsky, F.M. & Madiraju, S.R. Metabolic signaling in fuel-induced insulin secretion. *Cell Metab* **18**, 162-185 (2013).
15. Thorens, B., Guillam, M.T., Beermann, F., Burcelin, R. & Jaquet, M. Transgenic reexpression of GLUT1 or GLUT2 in pancreatic beta cells rescues GLUT2-null mice

from early death and restores normal glucose-stimulated insulin secretion. *J Biol Chem* **275**, 23751-23758 (2000).
16. Pliszka, M. & Szablewski, L. Glucose Transporters as a Target for Anticancer Therapy. *Cancers (Basel)* **13** (2021).
17. Peng, M. *et al.* Aerobic glycolysis promotes T helper 1 cell differentiation through an epigenetic mechanism. *Science* **354**, 481-484 (2016).
18. Chang, C.H. *et al.* Posttranscriptional control of T cell effector function by aerobic glycolysis. *Cell* **153**, 1239-1251 (2013).
19. Honjo, K., Yan Xu, X., Kapp, J.A. & Bucy, R.P. Evidence for cooperativity in the rejection of cardiac grafts mediated by CD4 TCR Tg T cells specific for a defined allopeptide. *Am J Transplant* **4**, 1762-1768 (2004).
20. Valujskikh, A., Lantz, O., Celli, S., Matzinger, P. & Heeger, P.S. Cross-primed CD8(+) T cells mediate graft rejection via a distinct effector pathway. *Nat Immunol* **3**, 844-851 (2002).
21. Lantz, O., Grandjean, I., Matzinger, P. & Di Santo, J.P. Gamma chain required for naive CD4+ T cell survival but not for antigen proliferation. *Nat Immunol* **1**, 54-58 (2000).
22. Karkeni, E. *et al.* Vitamin D Controls Tumor Growth and CD8+ T Cell Infiltration in Breast Cancer. *Front Immunol* **10**, 1307 (2019).
23. Thorens, B. GLUT2, glucose sensing and glucose homeostasis. *Diabetologia* **58**, 221-232 (2015).
24. Coimbra, I.B., Jimenez, S.A., Hawkins, D.F., Piera-Velazquez, S. & Stokes, D.G. Hypoxia inducible factor-1 alpha expression in human normal and osteoarthritic chondrocytes. *Osteoarthritis Cartilage* **12**, 336-345 (2004).
25. Hayashi, M. *et al.* Induction of glucose transporter 1 expression through hypoxia-inducible factor 1alpha under hypoxic conditions in trophoblast-derived cells. *J Endocrinol* **183**, 145-154 (2004).
26. Sacramento, J.F. *et al.* Insulin resistance is associated with tissue-specific regulation of HIF-1alpha and HIF-2alpha during mild chronic intermittent hypoxia. *Respir Physiol Neurobiol* **228**, 30-38 (2016).
27. Welsh, S., Williams, R., Kirkpatrick, L., Paine-Murrieta, G. & Powis, G. Antitumor activity and pharmacodynamic properties of PX-478, an inhibitor of hypoxia-inducible factor-1alpha. *Mol Cancer Ther* **3**, 233-244 (2004).
28. Christie, D.A., Kirchhof, M.G., Vardhana, S., Dustin, M.L. & Madrenas, J. Mitochondrial and plasma membrane pools of stomatin-like protein 2 coalesce at the immunological synapse during T cell activation. *PLoS One* **7**, e37144 (2012).

29. Chou, F.C., Shieh, S.J. & Sytwu, H.K. Attenuation of Th1 response through galectin-9 and T-cell Ig mucin 3 interaction inhibits autoimmune diabetes in NOD mice. *Eur J Immunol* **39**, 2403-2411 (2009).
30. Zhu, C. *et al.* The Tim-3 ligand galectin-9 negatively regulates T helper type 1 immunity. *Nat Immunol* **6**, 1245-1252 (2005).
31. Wu, C. *et al.* Galectin-9-CD44 interaction enhances stability and function of adaptive regulatory T cells. *Immunity* **41**, 270-282 (2014).
32. Selno, A.T.H. *et al.* Transforming growth factor beta type 1 (TGF-beta) and hypoxia-inducible factor 1 (HIF-1) transcription complex as master regulators of the immunosuppressive protein galectin-9 expression in human cancer and embryonic cells. *Aging (Albany NY)* **12**, 23478-23496 (2020).
33. Liu, J., Huang, S., Su, X.Z., Song, J. & Lu, F. Blockage of Galectin-receptor Interactions by alpha-lactose Exacerbates Plasmodium berghei-induced Pulmonary Immunopathology. *Sci Rep* **6**, 32024 (2016).
34. Ohtsubo, K. *et al.* N-Glycosylation modulates the membrane sub-domain distribution and activity of glucose transporter 2 in pancreatic beta cells. *Biochem Biophys Res Commun* **434**, 346-351 (2013).
35. Adler, J. & Parmryd, I. Colocalization analysis in fluorescence microscopy. *Methods Mol Biol* **931**, 97-109 (2013).
36. Ma, R. *et al.* A Pck1-directed glycogen metabolic program regulates formation and maintenance of memory CD8(+) T cells. *Nat Cell Biol* **20**, 21-27 (2018).
37. Mihout, F. *et al.* Acute metabolic acidosis in a GLUT2-deficient patient with Fanconi-Bickel syndrome: new pathophysiology insights. *Nephrol Dial Transplant* **29 Suppl 4**, iv113-116 (2014).
38. Xiong, L.J., Jiang, M.L., Du, L.N., Yuan, L. & Xie, X.L. Fanconi-Bickel syndrome in an infant with cytomegalovirus infection: A case report and review of the literature. *World J Clin Cases* **8**, 5467-5473 (2020).
39. Michau, A. *et al.* Mutations in SLC2A2 gene reveal hGLUT2 function in pancreatic beta cell development. *J Biol Chem* **288**, 31080-31092 (2013).
40. Martin, M.D. & Badovinac, V.P. Defining Memory CD8 T Cell. *Front Immunol* **9**, 2692 (2018).
41. Phan, A.T. *et al.* Constitutive Glycolytic Metabolism Supports CD8(+) T Cell Effector Memory Differentiation during Viral Infection. *Immunity* **45**, 1024-1037 (2016).
42. Cham, C.M., Driessens, G., O'Keefe, J.P. & Gajewski, T.F. Glucose deprivation inhibits multiple key gene expression events and effector functions in CD8+ T cells. *Eur J Immunol* **38**, 2438-2450 (2008).

43. van der Windt, G.J. *et al.* CD8 memory T cells have a bioenergetic advantage that underlies their rapid recall ability. *Proc Natl Acad Sci U S A* **110**, 14336-14341 (2013).
44. Sukumar, M. *et al.* Inhibiting glycolytic metabolism enhances CD8+ T cell memory and antitumor function. *J Clin Invest* **123**, 4479-4488 (2013).
45. Demetriou, M., Granovsky, M., Quaggin, S. & Dennis, J.W. Negative regulation of T-cell activation and autoimmunity by Mgat5 N-glycosylation. *Nature* **409**, 733-739 (2001).
46. Kumar, A., Xiao, Y.P., Laipis, P.J., Fletcher, B.S. & Frost, S.C. Glucose deprivation enhances targeting of GLUT1 to lipid rafts in 3T3-L1 adipocytes. *Am J Physiol Endocrinol Metab* **286**, E568-576 (2004).
47. Matarese, G., La Cava, A. & Horvath, T.L. In vivo veritas, in vitro artificia. *Trends Mol Med* **18**, 439-442 (2012).
48. Norata, G.D. *et al.* Effects of fractalkine receptor variants on common carotid artery intima-media thickness. *Stroke* **37**, 1558-1561 (2006).
49. Schwoebel, F., Barsig, J., Wendel, A. & Hamacher, J. Quantitative assessment of mouse skin transplant rejection using digital photography. *Lab Anim* **39**, 209-214 (2005).
50. Schreiber, E. *et al.* Astrocytes and glioblastoma cells express novel octamer-DNA binding proteins distinct from the ubiquitous Oct-1 and B cell type Oct-2 proteins. *Nucleic Acids Res* **18**, 5495-5503 (1990).